Macromolecules

ARTICLE

pubs.acs.org/Macromolecules

Isotactic Polypropylene with (3,1) Chain-Walking Defects: Characterization, Crystallization, and Melting Behaviors

Carolina Ruiz-Orta,[†] Juan P. Fernandez-Blazquez,[†] Amelia M. Anderson-Wile,[‡] Geoffrey W. Coates,[‡] and Rufina G. Alamo*[,†]

[†]Department of Chemical and Biomedical Engineering, FAMU-FSU College of Engineering, Tallahassee, Florida 32310, United States

[‡]Department of Chemistry and Chemical Biology, Baker Laboratory, Cornell University, Ithaca, New York 14853, United States

Supporting Information

ABSTRACT: Using two living nickel α-diimine complexes (*rac*-**1** and *rac*-**4**) activated with methylaluminoxane (MAO), isotactic polypropylene (*i*PP) samples containing five types of regiodefects were synthesized. Both isolated and successive groups of (2,1) and (3,1) enchainments were identified by solution-state ^{13}C NMR spectroscopy. The extended monomer and bulky nature of these defects add some restraints to the crystallinity level that can be achieved in these polymer samples. The complex based on a cumyl-derived ligand, *rac*-**4**, produces higher molecular weight *i*PP with a higher content of bulky defects than *rac*-**1**. Melting temperatures and crystallinity levels of *rac*-**4**-derived *i*PP are accordingly lower than the polymers obtained from *rac*-**1**. Although the nature of the chain-walking defect is similar to the addition of the ethylene unit, the difference in polymer properties is profound. At equivalent point defects per total monomers (X_B), *i*PP samples with chain-walking defects display lower melting temperatures and much lower degrees of crystallinity than random 1-alkene copolymers, including those with comonomers excluded from the crystal lattice such as the 1-hexene and 1-octene counits. Furthermore, *i*PP containing (3,1) regiodefects develops significantly higher contents of the γ-polymorph than any other *i*PP or random copolymer with a matched X_B composition. The experimental evidence is consistent with shorter crystallizable sequences for *i*PP with chain-walking defects based on (3,1) enchainments. Taking crystallizable and noncrystallizable total units as the basis to compute point defects, the properties of (3,1) *i*PP adhere to the basis of exclusion equilibrium theory, indicating that the defects are *random-bulky* or generated in a random fashion but of a defined extended/multimonomer nature.

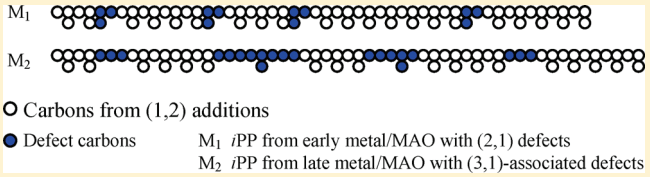

1. INTRODUCTION

The thermodynamic, structural, and mechanical properties of isotactic polypropylene depend strongly on the type, content, and distribution of defects [other than isotactic (1,2) additions] generated during synthesis. In the last 2 decades, the spectrum of new polyolefin materials exhibiting properties of highly crystalline thermoplastics to plastomers and elastomers has undergone an exponential expansion due to the development of metal coordination catalysts.[1−16] In particular, polypropylene materials have been developed ranging from statistically random copolymers to stereoblocky elastomeric types, which serve as examples of the ability of new synthetic strategies to tailor structures and properties of polyolefins by a suitable choice of the coordination catalyst precursor.[1−6] The availability of such a wide variety of materials has led to significant improvements in characterization of molecular microstructure,[17−23] which remains a main variable affecting properties.

Recently, a new family of polypropylene has been synthesized via living polymerization with late-metal nickel α-diimine catalysts. These polymers differ from polypropylene produced by early-metal catalysts due to chain-walking events that often result in unique defect microstructures.[16,24−28] Analysis of the amorphous polypropylene synthesized with Brookhart's nickel α-diimine catalyst by ^{13}C NMR spectroscopy proved to be quite complex. The catalyst produced moderately syndiotactic polymers with an array of defects generated by inversions and (3,1) enchainments as well as different types of short- and long-chain branches.[27,28] In 2005, Coates et al.[9] reported a living, chiral Ni(II) α-diimine catalyst capable of forming isotactic polypropylene as well as undergoing controlled chain walking when activated with MAO in the presence of propylene. An amorphous, regioirregular polymer was produced at higher reaction temperatures (T_{rxn} = 0 °C) while an isotactic, regioregular polymer was obtained at low reaction temperatures (T_{rxn} = −60 °C). Later modifications to the Ni(II) α-diimine catalyst resulted in a polymerization catalyst that maintained isotacticity while increasing the rate of polymerization.[29] Some recent studies capitalize on the ability of the living catalyst to generate intrachain blocks of stereoregular (hard) and regioirregular (soft) chain segments by alternating high and low reaction temperature. The melt-phase structure and mechanical properties can be tuned by the length and

Received: February 1, 2011
Revised: March 10, 2011
Published: April 05, 2011

Scheme 1. Schematic *i*PP Carbons with (2,1) Defects Generated by Early-Metal/MAO Catalysts (M_1) and Those Found in *i*PP Synthesized by Late-Metal/MAO Catalysts (M_2)[a]

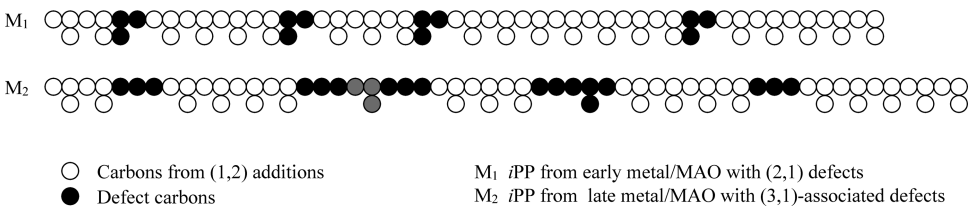

[a] M_2 includes isolated (3,1), alternating (3,1)(1,2)(3,1), and (3,1)(2,1) as examples of chain-walking defects. Note that for crystallization purposes the central (1,2) addition of the alternating (3,1)(1,2)(3,1) defect is considered a defected unit. M_1 and M_2 types of molecules are compared for an equivalent (25) number of monomers.

relative defect composition of the blocks.[30,31] Characteristic inversions and ethylene runs were initially identified from the ^{13}C NMR spectra of these polymers. The presence of backbone ethylene runs is a result of "chain-walking", in which the metal center migrates along the growing polymer chain through a series of β-hydride elimination and reinsertion events. To date, a detailed defect microstructure characterization of crystalline *i*PP produced with the nickel α-diimine catalysts prior to and after ligand modifications has not been carried out. Furthermore, in spite of the intense interest in the synthesis of polyolefins made with the late-transition-metal catalyst (Ni, Pd), their crystalline properties in reference to polypropylenes obtained with early-metal metallocenes or with classical Ziegler−Natta catalysts have not been studied. With complexes for the isotactic polymerization of propylene in hand, a detailed ^{13}C NMR study on polypropylene microstructure and crystalline properties was pursued.

The (3,1) enchainment is a distinctive feature of *i*PP with chain-walking defects resulting in extra CH_2 in the *i*PP backbone compared to defects generated by inversion or 1-alkene comonomers. The result is a chain straightening due to the extended length of the defect in the main chain, as shown in Scheme 1. Here, *i*PP backbones with (2,1) defects generated by early-metal/MAO catalysts and those found in *i*PP synthesized by late-metal/MAO catalysts are compared for an equivalent number of monomers. The schematic defect microstructure emphasizes the extension of the defects in the backbone (bulkier defects) and the shortening of isotactic sequence runs in *i*PP obtained with late-metal/MAO catalysts. Defects associated with (3,1) enchainments disrupt the 3_1 helical symmetry in a manner not found in *i*PP copolymers with ethylene or any other 1-alkene comonomer and are not expected to enter the crystalline regions to any significant extent. Accordingly, the *i*PP properties such as melting points, degree of crystallinity, and polymorphic behavior should differ depending on the relative content of short and long backbone defect units.

The effect of stereodefects and 1-alkene comonomers on the crystalline packing and melting behavior of *i*PP synthesized with early-metal metallocene catalysts is now well-understood from extensive work with these systems during the past decade. Due to the difficult nature of the synthesis, *i*PP with only regiodefects has been less studied. Furthermore, the crystallization and melting behaviors are complicated by the formation of different crystallographic polymorphs, which depend on the defect microstructure of the chain (composition and distribution) as well as crystallization conditions.[32−37] Most crystalline properties are directly affected by how the defect is partitioned between crystalline and noncrystalline regions.[38−42] The most commonly observed crystal phase is the monoclinic or α form. Increasing structural irregularities in the isotactic polypropylene chain either as stereo-, regio- ((2,1) type), or constitutional defects, such as a comonomer unit, induce the formation of an orthorhombic phase (γ) with unique packing features in the realm of crystalline polymers. The unit cell is formed of nonparallel bilayers tilted at 81° with respect to each other.[36] Studying 1-alkene *i*PP-based copolymers in a range of comonomer >10 mol % revealed packing characteristics specific to a given comonomer type that were not predicted from the studies in the low comonomer range.[41] For example, metallocene 1-hexene and 1-butene *i*PP copolymers with <10 mol % comonomer are di-isomorphic. They crystallize in a mixture of α (monoclinic) and γ (orthorhombic) phases. However, at comonomer contents >15 mol %, the 1-hexene units, which are not incorporated in the crystals at low levels, cocrystallize with the propene units in a more dense trigonal unit cell.[41,42] In contrast, the 1-butene units are easily incorporated in the crystals at all comonomer levels, causing expansion of the lattice. At contents >18 mol %, the expansion of the *a* axis of the α lattice from the butene incorporation is too large to allow the homoepitaxial growth of the γ polymorph. Hence, for >18 mol % comonomer, γ no longer develops in propylene−1-butene (PB) copolymers.[41] Conversely, the ethylene unit makes a small strain in α or in the γ lattice so that the latter is developed in copolymers with high contents of ethylene (up to 21 mol %).

The interest in studying the crystalline properties of (3,1) *i*PP made with late-metal nickel α-diimine catalysts stems from their unique microstructures and the fact that the properties of these materials are controlled to a large extent by the crystalline structure and the level of crystallinity acquired after melt processing. First of all, the defects generated by chain-walking (ethylene runs) are counits that confer a copolymeric character to the *i*PP chain. In addition to the content of defects, the inter- and intramolecular distribution of the defects as well as the partitioning of defects between crystalline and noncrystalline regions affect the melting and crystallization behavior of polypropylenes. Comparison of (3,1) *i*PP crystalline properties with those of random propylene−ethylene copolymers is of interest due to the generation in the novel *i*PP of backbone ethylene runs via (3,1) enchainments that are, in principle, of a similar nature to the ethylene runs resulting from propylene−ethylene copolymerization. Furthermore, if chain-walking defects are generated as random events and are excluded from the crystalline regions, their melting and crystalline properties should parallel the behavior of propylene−1-hexene (<13 mol % comonomer) and propylene−1-octene, since both counits are known to be excluded from the crystals.[40]

In this work, we evaluate comparatively the thermodynamic and crystalline properties of the novel *i*PP in reference to the

dx.doi.org/10.1021/ma200231a |*Macromolecules* 2011, 44, 3436–3451

behavior of polypropylene as well as *i*PP random copolymers produced by early-metal/MAO metallocene catalysts free of chain-walking defects. Of particular interest is the influence of the mole fraction of defects and the backbone length of the defect on the melting temperature, the level of crystallinity determined by X-ray diffraction and thermal analysis, the crystallite thickness, and the polymorphic behavior. For a direct comparison, the evaluation is carried out on the basis of point defects, defined as a single defect monomer or a multimonomer defect run bonded on either side by nondefect monomer runs.

2. EXPERIMENTAL SECTION

2.1. Polypropylene Synthesis. General Procedures. All manipulations of air- and/or water-sensitive compounds were carried out under dry nitrogen using Braun UniLab drybox or standard Schlenk techniques. Methylene chloride was purified over an alumina column and degassed by three freeze−pump−thaw cycles before use. Toluene was purified over columns of alumina and copper (Q5). Propylene (Airgas, research purity) was purified over columns (40 cm inner diameter × 120 cm long) of BASF catalyst R3-12, BASF catalyst R3-11, and 4 Å molecular sieves. MMAO-7 (7 wt % Al in Isopar E, Akzo Nobel) and MMAO-3a (7 wt % Al in heptane, Akzo Nobel) were used as received. PMAO-IP (13 wt % Al in toluene, Akzo Nobel) was dried in vacuo to remove residual trimethylaluminum and used as a solid white powder.

Scheme 2. Late-Metal α-Diimine Complexes Used in the Synthesis of *i*PP with Chain-Walking Defects

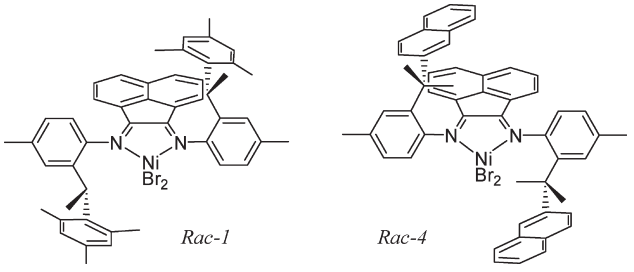

Rac-1 *Rac-4*

Complex Synthesis. Polymerization precatalysts with a mesityl ligand (*rac*-**1**) or cumyl ligand (*rac*-**4**) were prepared using previously reported methods (Scheme 2).[9,29]

Propylene Polymerization, Table 1, Entries 1 and 2. In a glovebox, a 6 oz (180 mL) round-bottom Laboratory Crest reaction vessel (Andrews Glass) was charged with toluene (25 mL) and a solution of MMAO-7 (2.4 mL, 4.6 mmol). The solution was cooled to −78 °C and propylene (15 g) was condensed into the vessel. The reaction mixture was then allowed to equilibrate to −55 °C. After 10 min, *rac*-**4** (0.016 g, 17 μmol) was injected as a solution in 2 mL of dry, degassed CH_2Cl_2. An aliquot was taken from the reaction mixture via cannula using an overpressure of 30 psig propylene after 6 h. The polymerization was quenched with methanol (10 mL) after 48 h. Both the aliquot and the final reaction mixture were precipitated into copious acidic methanol [5% HCl (aq)] and the resulting suspensions stirred overnight. Both polymers were isolated, dissolved in hot toluene, filtered over Celite/silica/alumina, precipitated with methanol, isolated again, and dried to constant weight in vacuo at 60 °C.

Propylene Polymerization, Table 1, Entries 3−7. In a glovebox, a 6 oz (180 mL) round-bottom Laboratory Crest reaction vessel (Andrews Glass) was charged with toluene (25 mL) and a solution of MMAO-7 (2.4 mL, 4.6 mmol). The solution was cooled to −78 °C and the appropriate mass of propylene was condensed into the vessel. The reaction mixture was then allowed to equilibrate to the desired temperature. After 10 min, *rac*-**4** (17 μmol) was injected as a solution in 2 mL of dry, degassed CH_2Cl_2. The polymerization was quenched with methanol (10 mL). The reaction mixture was then precipitated into copious acidic methanol [5% HCl (aq)] and the resulting suspension stirred overnight. The polymer was isolated, dissolved in hot toluene, filtered over Celite/silica/alumina, precipitated with methanol, isolated again, and dried to constant weight in vacuo at 60 °C.

Propylene Polymerization, Table 1, Entries 8−15. In a glovebox, a 6 oz (180 mL) round-bottom Laboratory Crest reaction vessel (Andrews Glass) was charged with toluene (25 mL) and a solution of MMAO-3A (2.5 mL, 4.6 mmol). The solution was cooled to −78 °C and an appropriate mass of propylene was condensed into the vessel. The reaction mixture was then allowed to equilibrate to the desired temperature. After 10 min, *rac*-**1** (0.018 g, 17 μmol) was injected as a solution in 2 mL of dry, degassed CH_2Cl_2. The polymerization was quenched with

Table 1. Polymerization Conditions of Polypropylene with (3,1)-Associated Regiodefects

complex	entry	polymer designation	*T* (°C)	time (h)	total defects (mol %)[c]	M_w (kg/mol)[d]	M_w/M_n[d]
rac-**4**	1[a]	*i*PP3.06	−55	48	3.06	71	1.23
rac-**4**	2[a]	*i*PP3.29	−55	6	3.29	41	1.18
rac-**4**	3[a]	*i*PP3.51	−55	48	3.51	100	1.39
rac-**4**	4[a]	*i*PP3.64	−50	48	3.64	209	1.35
rac-**4**	5[b]	*i*PP5.93	−40	48	5.93	216	1.32
rac-**4**	6[b]	*i*PP8.11	−35	48	8.11	273	1.30
rac-**4**	7[b]	*i*PP15.37	−30	24	15.37	294	1.33
rac-**1**	8[a]	*i*PP3.33	−55	48	3.33	19	1.46
rac-**1**	9[b]	*i*PP5.04	−50	48	5.04	19	1.34
rac-**1**	10[b]	*i*PP6.97	−48	42	6.97	30	1.25
rac-**1**	11[b]	*i*PP8.52	−46	47	8.52	44	1.21
rac-**1**	12[b]	*i*PP10.22	−45	46	10.22	44	1.15
rac-**1**	13[b]	*i*PP11.82	−43	44	11.82	81	1.15
rac-**1**	14[b]	*i*PP15.12	−40	24	15.12	60	1.14
rac-**1**	15[b]	*i*PP16.75	−35	20	16.75	66	1.14

[a] General Conditions: Ni = 17 μmol, [Al]/[Ni] = 270, 15 g of propylene. [b] General Conditions: Ni = 17 μmol, [Al]/[Ni] = 270, 5 g of propylene. [c] Determined using ^{13}C NMR spectroscopy in 1,1,2,2-tetrachloroethane-d_2 at 135 °C. [d] Molecular weight (M_w) and molecular weight distribution were determined by gel permeation chromatography at 140 °C in 1,2,4-trichlorobenzene.

dx.doi.org/10.1021/ma200231a |*Macromolecules* 2011, 44, 3436–3451

methanol (10 mL). The reaction mixture was then precipitated into copious acidic methanol [5% HCl (aq)] and the resulting suspension stirred overnight. The polymer was isolated, dissolved in hot toluene, filtered over Celite/silica/alumina, precipitated with methanol, isolated again, and dried to constant weight in vacuo at 60 °C.

2.2. Characterization Techniques. ^{1}H and ^{13}C NMR spectra of polymers were recorded using a Varian UnityInova (600 MHz) spectrometer equipped with a 10 mm broadband probe operating at 135 °C and referenced versus residual nondeuterated solvent shifts. The polymer samples were dissolved in 1,1,2,2-tetrachloroethane-d_2 (10 wt %) in a 5 mm o.d. tube, and spectra were collected at 135 °C. For quantitative proton decoupled ^{13}C NMR analysis, the spectra were collected in two spectrometers. A set was acquired in the same Varian UnityInova (600 MHz) spectrometer with inverse gated decoupling using the TYCO-25 decoupling sequence, a 30° excitation pulse width, 2.0 s acquisition time, and 30 s relaxation delay. Selected *i*PP samples were also analyzed at 120 °C in a 10 mm probe using a Varian spectrometer with a frequency of 700 MHz on ^{1}H. The conditions to obtain the latest spectra were as follows: a 90° pulse, an acquisition time adjusted to give a digital resolution between 0.1 and 0.12 Hz, and >10 s pulse acquisition delay time with continuous broadband proton decoupling. Swept square wave modulation without gating was used during the entire acquisition period. The spectra were acquired using time averaging to provide a signal-to-noise level adequate to measure the signals of interest. Samples were dissolved in tetrachloroethane-d_2 at concentrations between 10 and 15 wt % prior to being inserted into the spectrometer magnet. Spectra were referenced by setting the mmmm methyl signal to 21.83 ppm. Carbon multiplicity was determined in the same 700 MHz spectrometer using DEPT (distorsionless enhancement by polarization transfer) experiments.

Molecular weights (M_n and M_w) and polydispersities (M_w/M_n) were determined by high-temperature gel permeation chromatography (GPC). Analyses were performed with a Waters Alliance GPCV 2000 GPC equipped with a Waters DRI detector and viscometer. The column set (four Waters HT 6E and one Waters HT 2) was eluted with 1,2,4-trichlorobenzene containing 0.01 wt % di-*tert*-butylhydroxytoluene (BHT) at 1.0 mL/min at 140 °C. Data were calibrated using monomodal polyethylene standards (from Polymer Standards Service).

The original powders were placed on rectangular 10 × 5 × 0.25 mm stainless steel frames and sandwiched between thin Teflon films by melt compression in a Carver press at 180−200 °C (5 min, 1380 KPa). The hot plates were then taken to room temperature and left at ambient conditions for at least 2 weeks prior to recording the first DSC melting. Since some of the *i*PP samples have slow crystallization kinetics at room temperature, a relatively long aging allows comparison of the melting behavior among the series at a stage when most of the *i*PP crystalline structure has evolved. Nonisothermal melting and crystallizations (10 °C/min) were carried out using a differential scanning calorimeter Perkin-Elmer DSC-7 under nitrogen flow. Temperature and heat flow calibrations were performed with indium as standard. Isothermal crystallizations were carried out either in the DSC or in controlled temperature baths. To maximize heat transfer, the DSC was operated in conjunction with an intracooler and under dry nitrogen flow. For the DSC experiments, the films were melted at 180 °C for 3 min and cooled at 40 °C/min to the required crystallization temperature.

Wide- and small-angle X-ray diffractograms (SAXS, WAXD) were obtained at ambient temperature on samples that were previously isothermally crystallized either in the DSC or in thermostated baths using a Bruker Nanostar diffractometer with a IμS microfocus X-ray source and equipped with a HiStar 2D Multiwire SAXS detector and a Fuji Photo Film image plate for WAXD detection. The plates were read with a Fuji FLA-7000 scanner. SAXS profiles were calibrated with silver behenate and WAXD patterns with corundum; both standards were obtained from Bruker. The peak assignments for α and γ phase followed those given by Brückner and Meille[43] and Turner-Jones.[44] The fractional content of the γ form was calculated, after subtraction of the amorphous halo, from the areas of the reflection at 2θ = 20.1° characteristic of γ form and the reflection of α form at 2θ = 18.8°, as $A_\gamma/(A_\gamma + A_\alpha)$.[32] Peak fitting to mixed Gaussian and Lorentzian shapes was carried out with GRAMS. Crystallinity content derived by WAXD was evaluated from the X-ray powder diffraction profiles by the ratio between the crystalline diffraction area and the total area of the diffraction profile.

3. RESULTS AND DISCUSSION

3.1. Defect Microstructure Characterized by ^{13}C NMR Spectroscopy. The chain-walking defect microstructure of polypropylene synthesized with living Ni(II) α-diimine-based catalysts is known to be very complex.[27,28] Although Brookhart's early generation Ni(II) α-diimine catalysts were living, they produced basically amorphous, atactic polypropylene. Subsequent work by Coates et al.[9,29] showed that C_2-symmetric, living Ni(II) α-diimine catalysts, such as those of Scheme 2, exhibit a strong temperature dependence in the number and type of defects generated during polymerization of propene. At very low temperatures (−78 °C), they produce highly regioregular, isotactic polypropylene, whereas at higher reaction temperatures (0 °C), the catalysts produce regioirregular *i*PP with (3,1) enchainments. This (3,1) error occurs when propylene is inserted in a (2,1) fashion followed by a β-hydrogen elimination and reinsertion, the so-called chain-walking mechanism which is shown for illustrative purposes in Scheme 3. The (3,1) errors may occur in several forms including (Scheme 4) being isolated between (1,2) additions, alternating with (1,2) additions, as diads or triads [successive (3,1) defects], or followed or preceded by (2,1) inversions. In addition, tacticity errors and (2,1) inversions free of chain-walking may be also present. Due to the range of possible errors, a large variety of well-defined defect structures are feasible in controlled concentrations by changing the reaction temperature.

The analysis of the thermodynamic and structural properties of polypropylene with (3,1)-associated defects hinges on detailed microstructural characterization and quantitative analysis of all defects generated during polymerization and on their partitioning between crystalline and noncrystalline regions upon crystallization. Therefore, as a first step of our investigation the defects present in the polypropylene synthesized with *rac*-**1** and *rac*-**4** (Scheme 2) were identified and quantified by ^{13}C NMR. For the purpose of analyzing polypropylene crystallization behavior, each defected sequence flanked by isotactic runs is considered a defect unit (or a point defect). Due to the controlled but large variety of defect structures, in this work a defect sequence of any length that exhibits (3,1) enchainments is often referred as a (3,1)-associated defect.

A representative ^{13}C NMR spectrum of the polypropylene synthesized with C_2-symmetric, living Ni(II) α-diimine catalysts is shown in Figure 1 for *rac*-**1** *i*PP11.82. All other spectra of *i*PP obtained either from *rac*-**1** or *rac*-**4** display the same number of resonances, differing from the spectrum shown in Figure 1 only in their relative intensity. On the basis of the observed similarities in the ^{13}C NMR spectra, we concluded that both catalysts insert the same types of defects. Listed adjacent to the structures of Scheme 4 are the chemical shifts of each error type following prior assignments[9,27,28,45−50] and the terminology for the indicated carbons that was given by Carman et al.,[51] where S, T, and P refer to secondary (methylene), tertiary (methine), and primary

Scheme 3. Mechanism of (3,1) Defect Formation in Isotactic Polypropylene

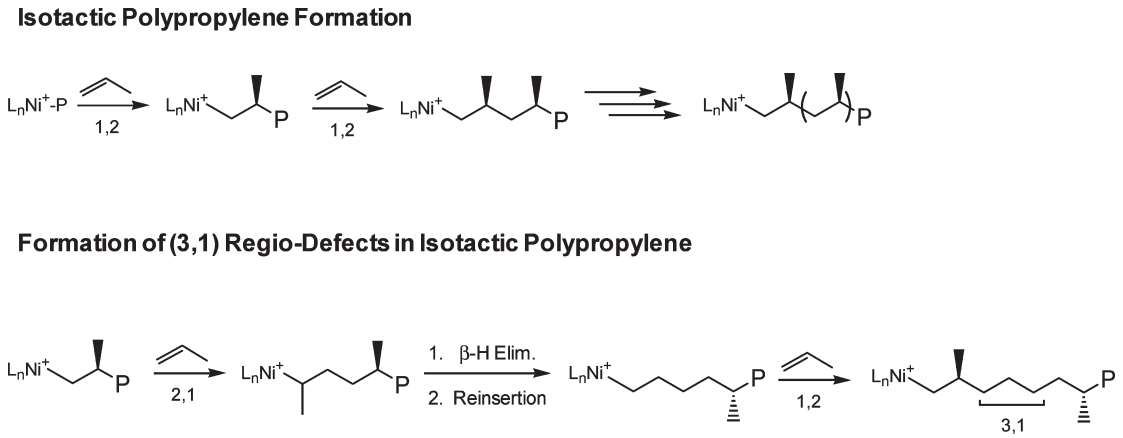

Scheme 4. Letter Designations Made for Pertinent Chain Defect Structures and Their ^{13}C NMR Peak Assignments[a]

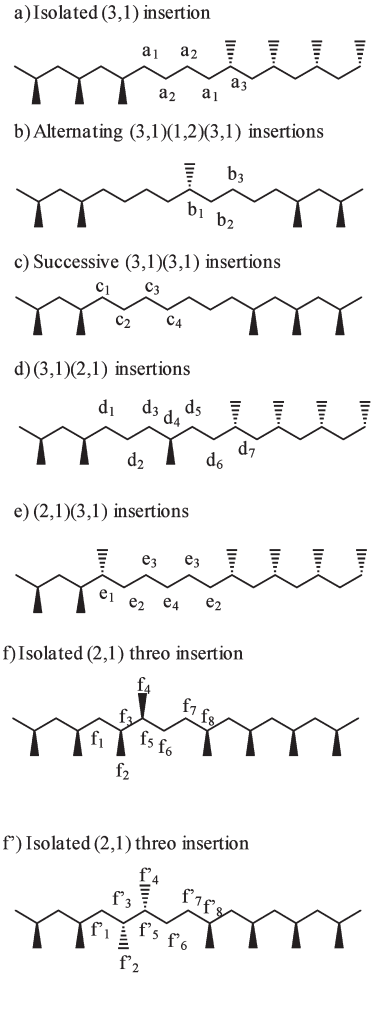

Shift, pep

$a_1 = 37.4$ ($S_{\alpha\delta}$)
$a_2 = 27.5$ ($S_{\beta\gamma}$)
$a_3 = 30.8$ ($T_{\beta\delta}$)

$b_1 = 33.2$ ($T_{\delta\delta}$)
$b_2 = 37.5$ ($S_{\alpha\delta}$)
$b_3 = 27.7$ ($S_{\beta\gamma}$)

$c_1 = 37.6$ ($S_{\alpha\delta}$)
$c_2 = 27.3$ ($S_{\beta\delta}$)
$c_3 = 30.3$ ($S_{\gamma\delta}$)
$c_4 = 29.9$ ($S_{\delta\delta}$)

$d_1 = 37.9$ ($S_{\alpha\delta}$)
$d_2 = 24.5$ ($S_{\beta\beta}$)
$d_3 = 38.5$ ($S_{\alpha\delta}$)
$d_4 = 33.5$ ($T_{\gamma\delta}$)
$d_5, d_6 = 34.2$-36 ($S_{\alpha\beta}$)
$d_7 = 31.2$ ($T_{\beta\gamma}$)

$e_1 = 38.5$ ($T_{\alpha\delta}$)
$e_2 = 37.5$ ($S_{\alpha\delta}$)
$e_3 = 27.5$ ($S_{\beta\delta}$)
$e_4 = 30.85$ ($S_{\gamma\gamma}$)

$f_1 = 43.58$ ($S_{\alpha\alpha}$)
$f_2 = 15.73$ ($P_{\alpha\beta}$)
$f_3 = 34.7$ ($T_{\alpha\beta}$)
$f_4 = 14.5$ ($P_{\alpha\gamma}$)
$f_5 = 37.01$ ($T_{\alpha\gamma}$)
$f_6 = 32.6$ ($S_{\alpha\beta}$)
$f_7 = 35.5$ ($S_{\alpha\beta}$)
$f_8 = 31.09$ ($T_{\beta\gamma}$)

$f'_1 = 43.29$ ($S_{\alpha\alpha}$)
$f'_2 = 15.05$ ($P_{\alpha\beta}$)
$f'_3 = 34.64$ ($T_{\alpha\beta}$)
$f'_4 = 15.46$ ($P_{\alpha\gamma}$)
$f'_5 = 38.77$ ($T_{\alpha\gamma}$)
$f'_6 = 32.38$ ($S_{\alpha\beta}$)
$f'_7 = 35.46$ ($S_{\alpha\beta}$)
$f'_8 = 31.27$ ($T_{\beta\gamma}$)

[a] Isolated (2,1) insertions are present in two different diastereoisomeric forms (f and f′). Note that with respect to the growing chain, and in accordance with Scheme 3, consecutive "errors" are listed beginning with the last and ending with the first erroneous insertion.

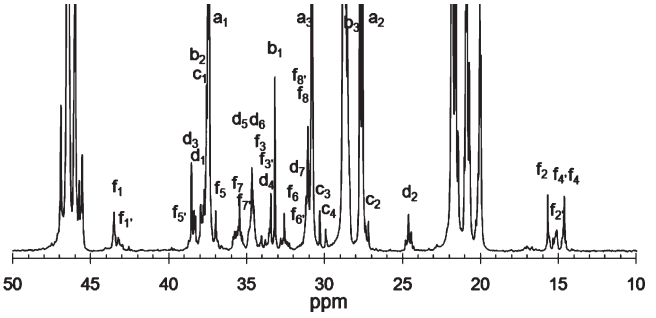

Figure 1. ^{13}C NMR spectrum of *i*PP 11.82 in 1,1,2,2-tetrachloroethane-d_2 at 135 °C.

(methyl) carbons, respectively; the Greek subscripts refer to the distance a given carbon is from a neighboring branched methine.

Defects of the types a, b, and c that were previously identified in the *i*PP made with the same catalysts (*rac*-**1** and *rac*-**4**) utilized in this study[9] are clearly present in all spectra. Defects of type d and the two conformational diastereoisomers, types f and f′, were not identified in ref 9 but are also present. The ^{13}C NMR DEPT spectra demonstrated that there are no methine carbons in the region of 38.5 ppm (carbon e_1 in Scheme 4) and hence rule out the generation of sequences type e by these catalysts. Furthermore, errors due to tacticity in the (1,2) additions were also considered.[9,27,52] Since the mmrr pentad is the best-resolved resonance in these spectra, the area around 21.05 ppm was integrated for quantitative purposes. Unusual short and long branches of the type observed with Pd and earlier Ni catalytic systems[27,28] were not found here. (For a detailed ^{13}C NMR chemical shift assignment, DEPT spectra, and quantitative analysis, we refer to the Supporting Information). Compositions of each defect type and total point defect composition per 100 monomers (X_B) are listed in Table 2 for the two *i*PP series studied.

The regiochemistry of *i*PP produced by these Ni(II) α-diimine complexes shows an interesting catalyst dependence that can be correlated with previously described differences in catalyst activity.[29] As expected, molecular weight and activity were observed to increase with reaction temperature (Table 1) for both complexes. Under the same conditions, the activity of *rac*-**4** (given by the variation of the molecular weight in the series) is much higher

Table 2. Point Defect Composition per 100 Monomers of Polypropylene with (3,1)-Associated Regiodefects

			regiodefects					
complex	polymer	stereodefects (mol %)[a]	a (mol %)	b (mol %)	c (mol %)	d (mol %)	f + f′ (mol %)	total defects (X_B) (mol %)
rac-**4**	*i*PP3.06	0.6	1.04[a]	0.22	0.00	0.78	0.42	3.06
rac-**4**	*i*PP3.29	0.5	1.12[a]	0.49[a]	0.00	1.18	0.00	3.29
rac-**4**	*i*PP3.51	0.6	0.84[a]	0.55[a]	0.00	1.52	0.00	3.51
rac-**4**	*i*PP3.64	0.6	1.27	0.28	0.14	1.05	0.30	3.64
rac-**4**	*i*PP5.93	0.6	3.06	0.60	0.00	1.67	0.00	5.93
rac-**4**	*i*PP8.11	0.7	3.22	0.63	0.18	3.22	0.16	8.11
rac-**4**	*i*PP15.37	0.8	4.56	2.22	1.31	5.66	0.82	15.37
rac-**1**	*i*PP3.33	0.8	2.53	0.00	0.00	0.00	0.00	3.33
rac-**1**	*i*PP5.04	0.7	2.58	0.48	0.00	0.00	1.28	5.04
rac-**1**	*i*PP6.97	0.6	4.07	0.82	0.08	0.00	1.40	6.97
rac-**1**	*i*PP8.52	0.5	5.00	1.02	0.08	0.00	1.92	8.52
rac-**1**	*i*PP10.22	0.5	7.15	1.41	0.15	0.00	1.01	10.22
rac-**1**	*i*PP11.82	0.5	6.16	2.13	0.48	1.15	1.40	11.82
rac-**1**	*i*PP15.12	0.7	7.16	2.96	0.00	2.67	1.63	15.12
rac-**1**	*i*PP16.75	0.6	8.93	3.26	1.06	1.69	1.21	16.75

[a] Data with 30−40% uncertainty. All other values have <10% uncertainty.

than that of *rac*-**1**, which is consistent with previous reports.[29] We also observe a progressive increase in the total defect content for both catalysts as temperature increases; however, there are large differences in the content of point defects generated by each catalyst at a fixed temperature (Figure 2). At the lowest temperatures, ≤−50 °C, both catalysts insert about the same low level of defects, whereas at ≥−50 °C the cumyl-derived catalyst (*rac*-**4**) is more isoselective, inserting fewer defects than *rac*-**1**. This difference remains even if instead of point defects a−f the content of defected monomers is evaluated vs reaction temperature. Since all defects (except stereodefects) derive from (2,1) insertions, it appears that the bulkier nature of the catalyst makes the (2,1) addition of propylene more difficult for the cumyl catalyst than for the mesityl catalyst.

Differences in the activity of each catalyst with respect to the insertion of a particular type of defect are analyzed by plotting the content of each defect over the total point defect content (Figure 3). For both catalysts, the variation of defects b, c, and f is similar, while major differences are found for defects a and d. For a fixed overall defect content, the *i*PP synthesized with *rac*-**1** contains more isolated (3,1) enchainments and negligible contents of type d defects. In contrast, *i*PP synthesized with *rac*-**4** inserts a very large number of d defects (∼35%). Due to the higher activity of *rac*-**4**, it appears that fewer (2,1) additions and subsequent chain-walking events are observed. Following a (2,1) misinsertion, a second (2,1) unit can then be added with high probability to undergo (3,1) enchainment, producing high contents of the d type sequence.

For a matched defect composition, runs of continuous isotactic sequences in *rac*-**4** *i*PP are on average shorter than in *rac*-**1** *i*PP due to greater type d defect content. This difference is quantitatively assessed by computing the number average isotactic run length between any two structural irregularities (N_{iso}).[53] N_{iso} is evaluated in Figure 4 in reference to the value of a control polypropylene chain with an equivalent content of randomly generated single monomer defect units. For a random distribution and infinite molecular weight, N_{iso} is approximated as the number of crystallizable isotactic monomers over the molar

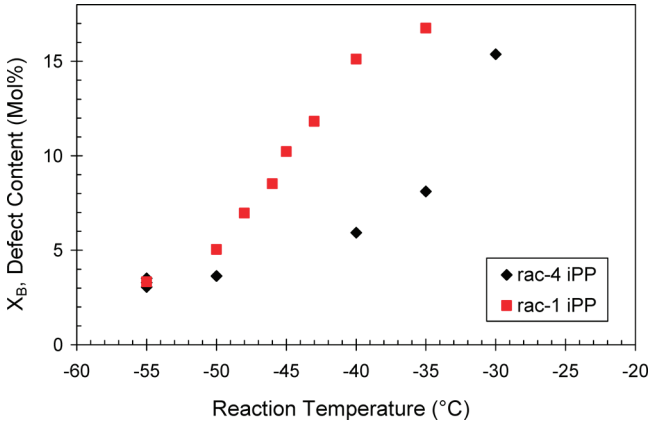

Figure 2. Effect of polymerization temperature on total defect content (mol %) in *i*PP synthesized with *rac*-**1** and *rac*-**4**.

defect composition or content of point defects (X_B). For (3,1)-associated defects, the fraction of isotactic monomers is found from the NMR data of Table 2 and the number of monomer units per point defect. The fraction of defect monomers in the control was obtained from X_B assuming a Bernoullian probability of monomer defects to compute the content of diads and triads.

In reference to the control, main-chain bulky defects such as b, c, and d (Table 2) insert up to 10 additional defect monomers per 100 total monomers. The contribution to shortening the average isotactic run length is up to one monomer in the series or up to 10% (*rac*-**1**) or 13% (*rac*-**4**) monomers shorter than for the control (Figure 4a). Figure 4b shows that the content of backbone crystallizable carbons out of 100 backbone carbons is even lower in these *i*PPs, as shown in Scheme 1. The (3,1) enchainment adds three defect carbons per monomer to the backbone, instead of two added by the most commonly studied defects [mrrm stereo, (2,1), or 1-alkene comonomer], which causes up to 20% reduction in the content of crystallizable backbone carbons with respect to *i*PP control. At a defect level of ∼12 mol %

dx.doi.org/10.1021/ma200231a |*Macromolecules* 2011, 44, 3436–3451

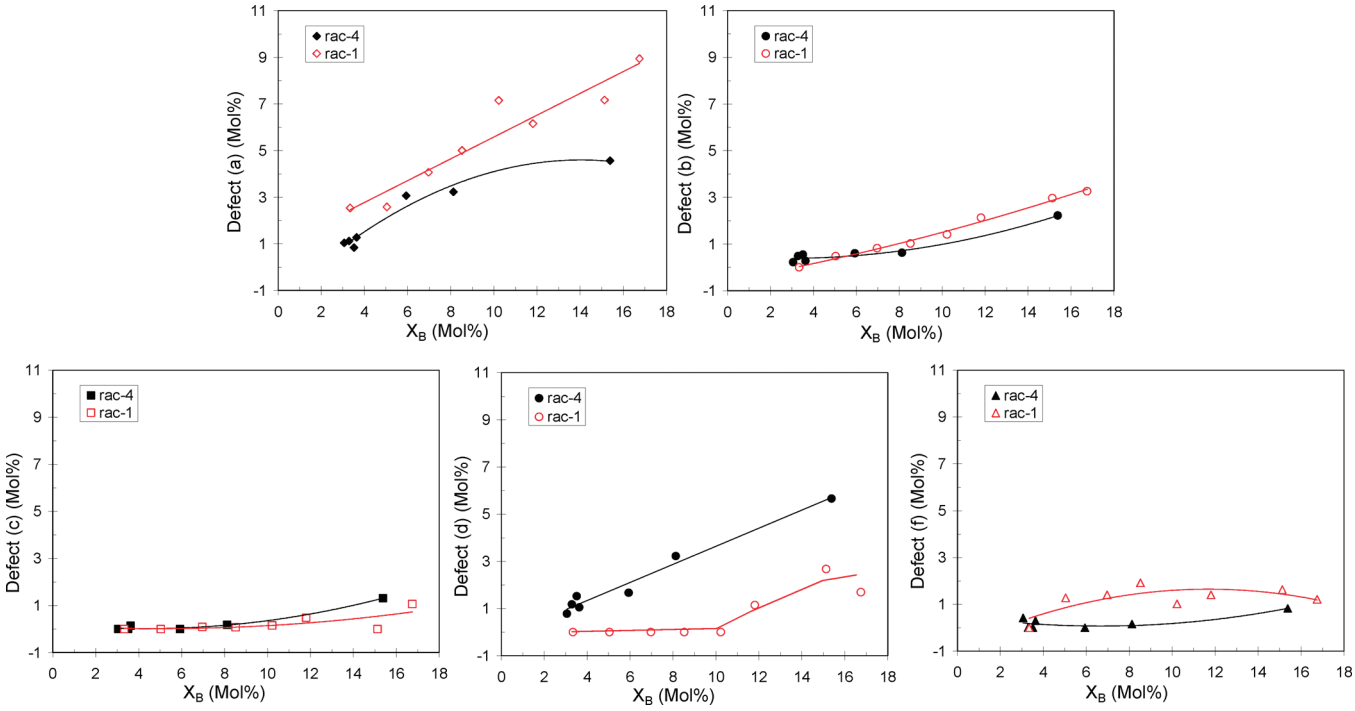

Figure 3. Plots of content of specific type of defect a, b, c, d, or f according to Scheme 4 vs total defect content (mol %) for *i*PP synthesized with *rac*-**1** and *rac*-**4**.

(Figure 4b), the number of crystallizable backbone carbons decreases from 87 in the control to about 75 carbons for a (3,1) *i*PP. This is quite a significant difference that becomes larger with increasing X_B.

The percent difference in shortening N_{iso} and backbone crystallizable carbons with respect to the *i*PP control is larger for *rac*-**4** than for the *rac*-**1** *i*PP, as seen in Figure 4a,b. This difference follows expectations from a larger content of d sequences in *rac*-**4** *i*PP that add two defect monomers and five backbone defect carbons. Thus, the combined analysis of the molar mass data and NMR defect microstructure point out that while *rac*-**4** is a more efficient catalyst than *rac*-**1** for isoselective propylene polymerization, on average, the defects generated by *rac*-**4** lead to shorter crystallizable sequence lengths compared to those generated by *rac*-**1**. These chain-walking defects based on (3,1) enchainments should effect melting and crystalline properties of *i*PP in reference to *i*PP with shorter backbone defects.

3.2. Melting Temperatures. We initially examined the influence of point defect concentration on the melting behavior determined by DSC of melt-pressed specimens that were kept at room temperature for approximately 2 weeks. Figure 5 shows the endotherms for both (3,1) *i*PP series compared with the endotherms of propylene−ethylene random copolymers (PE) in the same defect range. The PE copolymers were synthesized with an early metallocene catalyst and their crystalline and melting properties studied in prior works.[39,40] A direct comparison with PE copolymers is first made due to the similarity between the chain-walking defect and the addition of ethylene units. Furthermore, the copolymerization with ethylene using a metallocene catalyst and the (3,1) enchainment given by the living catalyst are expected to follow random statistics consistent with a site-control polymerization.[29,39] Hence, (3,1) *i*PP can be treated as a random copolymer where the a, b, c, d, f, and stereodefects are counits disrupting the isotactic chain regularity similar to the ethylene units in the PE. Comparing the shape of the endotherms of Figure 5, we conclude that except for a more pronounced aging (indicated by a melting peak at ~40 °C), the melting traces of (3,1) *i*PP and the PE are very similar.

Two melting peaks are observed for most copolymers; the highest melting peak decreases with increasing defect content and merges with the low melting peak at high comonomer concentration. The lowest melting peak is basically invariant with defect content and is associated with melting of thin, micelle-like crystallites that develop as a secondary crystallization in the intercrystalline regions during aging.[39,54] Essentially, the crystallization follows a crystalline sequence selection process, where the longest crystallizable sequences participate in the primary crystallization, while shorter sequences and noncrystallizable counits remain in the intercrystalline regions. With increasing defects, the concentration of sequences rejected to the intercrystalline region is higher, and the aging process is more pronounced, as indicated in the thermograms by a larger area of the low temperature peak. As the defect content reaches ≥15 mol %, the primary crystallization kinetics at ambient temperature becomes rather slow, such that the single endotherm reflects melting of isothermally formed crystallites at 23 ± 1 °C.[39] The major difference between PE and (3,1) *i*PP samples are lower melting temperatures and more prominent aging peaks in (3,1) *i*PP, all indicative of less crystalline materials than PE of equivalent defect composition.

In earlier works the melting and crystalline properties of random propylene−1-alkene copolymers were evaluated as a function of comonomer content, which is customarily obtained from ^{13}C NMR spectroscopy by adding the content of centered ethylene triads.[39−41] However, the multiplicity of counits and type of defects in *i*PP with chain-walking precludes a similar triad analysis. In order to evaluate the melting of (3,1) *i*PP and of random PE copolymers on the same compositional

basis, the point defect content for copolymers was recalculated from the relationship, $X_B = [PDP] + 0.5[PDD]$, where D is the comonomer unit. In this expression, runs of [DDD] and longer are counted by 0.5[PDD], since each segment of [DDD] is defined by the [DDP] triad at either end of the sequence. The contents of stereodefects and (2,1) defects are added to the above expression to compute the total X_B for the copolymers.

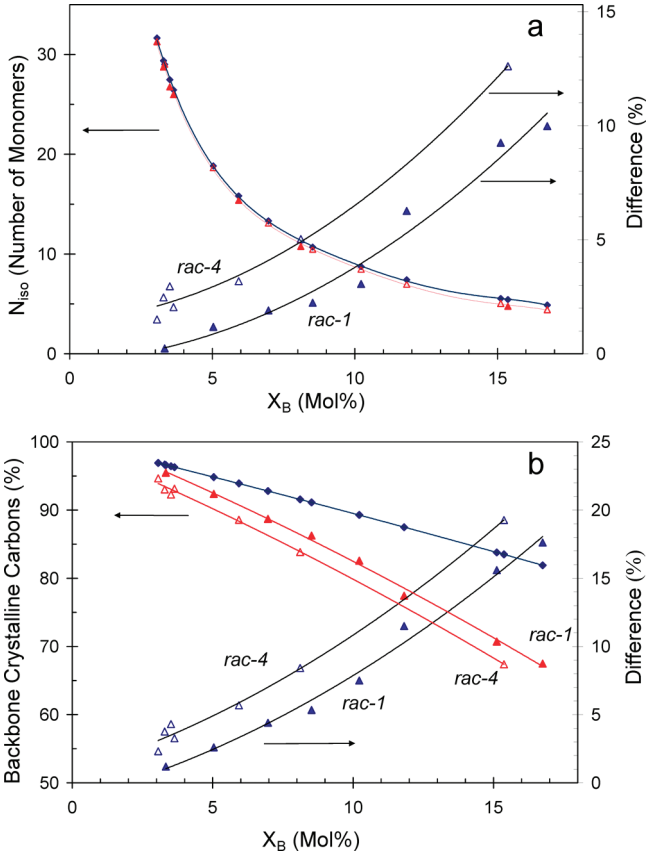

Figure 4. (a) Average isotactic sequence run length for (3,1) *i*PP of Table 2 (red triangles) and for analogs of *i*PP control with single monomer defects (diamonds). Right *y* scale shows percentage difference between values of N_{iso} for (3,1) *i*PP and *i*PP control. (b) Percentage backbone crystalline carbons (out of 100 backbone carbons) for (3,1) *i*PP of Table 2 (red triangles) and for control analogs of *i*PP (diamonds). Right *y* scale shows percentage difference between backbone crystalline carbons for (3,1) *i*PP and *i*PP control.

The high-temperature melting peak (T_{mp})—point defect composition relations of (3,1) *i*PP are compared in Figure 6 with data for random propene—1-alkene copolymers. In addition to PE, data for propylene—1-butene (PB), propylene—1-hexene (PH), and propylene—1-octene (PO) from our prior work[50] are also shown. As a reference homopolymer with low defect content, the melting temperature of an *i*PP synthesized with an early metallocene catalyst is also added (M*i*PP0.41). This *i*PP has M_w = 200 500 g/mol, M_w/M_n = 2.0, and 0.41 mol % defects of which 0.40% are (2,1) inversions and 0.01% mrrm stereo. All copolymers have similarly low contents of stereodefects and (2,1) defects to ensure that the change in melting temperature reflects mainly the variation in content and type of comonomer. Prior to melting, all specimens were subjected to the same thermal history as the (3,1) *i*PP. Changes in melting temperatures among the copolymers at a fixed composition are known to be due to differences in the partitioning of the counit between crystalline and noncrystalline regions.[39−41] PBs melt at the highest temperatures because the comonomer participates in the crystallites at the highest content; thus, their crystallizable sequences are the longest. The ethylene unit is also able to cocrystallize with the propylene units, but at a lower extent than is the 1-butene counit; this is reflected in PE melting temperatures

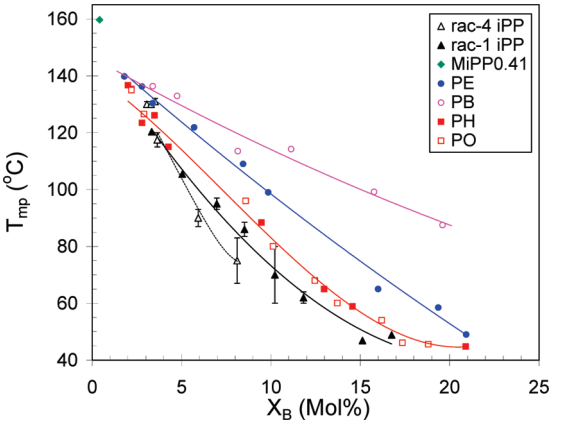

Figure 6. Melting temperature (T_{mp})—defect composition relations (X_B) for random propylene—1-alkene copolymers and for *i*PP with chain-walking defects. Data for copolymers are from ref 40. The melting of a low-defect early metallocene-made homopolymer (M*i*PP0.41) is also added as reference. The continuous and discontinuous lines are added only as guides of the variation of experimental data.

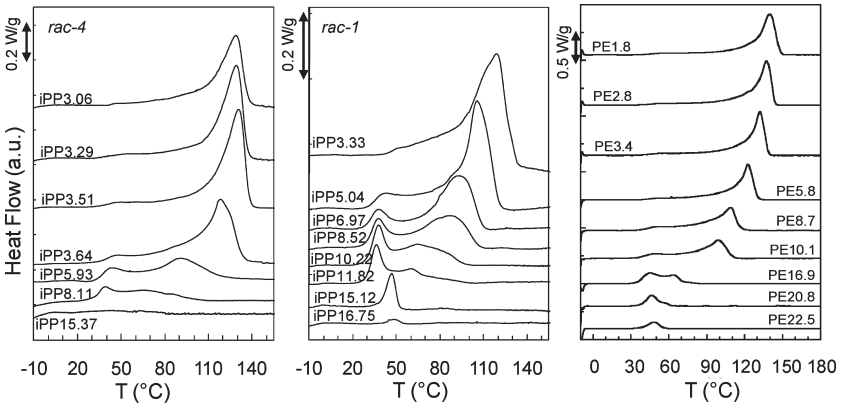

Figure 5. DSC endotherms of samples melt crystallized at ambient temperature (23 ± 2 °C) and kept at room temperature for ~2 weeks.

dx.doi.org/10.1021/ma200231a |*Macromolecules* 2011, 44, 3436–3451

lower than PBs, yet both are higher than matched PHs and POs. Lower melting of all POs and PHs with <13 mol % 1-hexene are due to the rejection of the counits from the crystallites;[40,41] their crystallizable sequences are shorter than those of PE or PB and their melting temperatures significantly lower.

Solid-state NMR studies of metallocene *i*PP with (3,1) defects indicate that this defect is rejected from the *i*PP crystallites.[38b] On this basis, one expects the (3,1) enchainment and larger defects, such as the b, c, and d types, to be also rejected. The same applies to the threo (2,1) defect (type f). The latter assessment is made on the basis of the large discrimination against entering the lattice for the (2,1) erythro defect.[38b] As the (3,1) defects are excluded from the crystallites, the initial expectation is for lower melting temperatures of (3,1) *i*PP with respect to PE, which is observed. Conversely, one expects the same melting temperature−defect composition behavior for (3,1) *i*PP and for PO and PH that have counits also excluded. However, the data of Figure 6 show that the melting temperatures of *i*PP with (3,1) enchainments are lower than the temperatures of PO or PH. The difference in melting increases with increasing concentration of (3,1) defects. For *i*PP produced with *rac*-**1**, the melting gap is only about 2 °C at a defect concentration of ∼3.5 mol % and becomes >10 °C at the highest defect contents. Except for three *rac*-**4** *i*PP samples in the low-concentration range that appear anomalously high in this plot (T_{mp} ∼ 130 °C), the T_{mp}−composition of *rac*-**4** *i*PP is displaced at even lower values. Lower melting temperatures for *rac*-**4** *i*PP reflect shorter isotactic sequence lengths that are explained by the higher concentration of long backbone defects. As revealed by the thermograms of Figure 5 and error bars in Figure 6, in the composition range from 8 to 10 mol %, the melting temperatures are subject to large uncertainties due to broad endotherms. It could be questioned if the difference in melting between *rac*-**1** and *rac*-**4** is caused by this uncertainty. Moreover, lower melting temperatures for *rac*-**4** *i*PP are supported by the thermal behaviors of *rac*-**1** *i*PP16.75 and *rac*-**4** *i*PP15.37. While *rac*-**1** *i*PP16.75 melts at 49 °C, *rac*-**4** *i*PP15.37 does not crystallize in spite of having lower defect content. In fact, all attempts to crystallize *rac*-**4** *i*PP15.37 at room temperature (23 °C) or lower for extended periods were unsuccessful.

If the final melting temperatures are plotted instead of T_{mp} in Figure 6 to reflect a composition of the melt surrounding the crystallites that resembles more closely the defect chain composition,[55] the melting difference between (3,1) *i*PP and PO or PH copolymers remain unchanged. We also considered if the difference in molecular weights between the *rac*-**1** and *rac*-**4** *i*PP as well as with the copolymers could explain the observed difference in melting in Figure 6. It has been shown that the melting temperatures of random ethylene copolymers decrease by 4−5 °C with increasing molecular weight in a range between 20 000 and 100 000 g/mol and remain basically unchanged for M_w > 100 000 g/mol.[56,57] The PH and PO copolymers have 90 000 < M_w < 150 000 while the *rac*-**1** *i*PP series has 20 000 < M_w < 80 000. With this variation in M_w, one would have expected higher, not lower, melting temperatures for *rac*-**1** *i*PP. Thus, the lower molecular weight of *rac*-**1** *i*PP cannot explain the displacement to lower values of the melting composition relation. In contrast, the higher molar mass of *rac*-**4** *i*PP series with respect to the *rac*-**1** *i*PP could partially explain the depression in melting temperatures for the *rac*-**4** *i*PP samples with relatively high defect content. Moreover, the observed 10 °C depression in melting temperature is much larger than anticipated. Furthermore, it does not explain how the *rac*-**4** *i*PP3.64 melting point, also with high molar mass

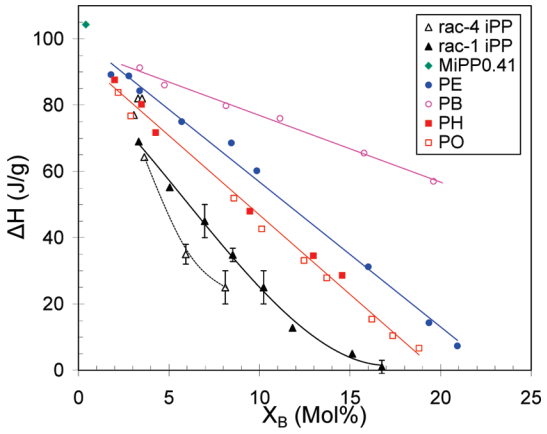

Figure 7. Heat flow−defect composition relations for random propylene−1-alkene copolymers and for *i*PP with chain-walking defects. The heat of fusion of a low-defect early metallocene-made homopolymer (M*i*PP0.41) is also added as reference. The continuous lines are added only as guides of the variation of experimental data.

(M_w = 209 000 g/mol), falls in line with the data of *rac*-**1** at a matched composition. Hence, it appears that the displacement of the melting temperature−composition relationship of *rac*-**1** *i*PP with respect to PH and PO, as well as *rac*-**4** *i*PP with respect to *rac*-**1**, has the same origin. Lower melting temperatures must be associated with the shortening of crystallizable sequences due to the multimonomer nature of b, c, and d defects as well as the extension of backbone defect carbons from (3,1) enchainments. Both effects will be accounted for and discussed later in the context of equilibrium theory for random copolymers.

3.3. Degree of Crystallinity. Next, we analyze the variation of (3,1) *i*PP heat of fusion (*y* axis) in a conventional plot (Figure 7) where the *x* axis is X_B (moles of point defects per 100 moles of monomer units). For comparison, data for random 1-alkene copolymers from our prior work are also shown.[40] PH copolymers with >15 mol % l-hexene are not displayed, due to their propensity to develop a trigonal denser polymorph and exhibit higher heat of fusion due to the inclusion of the l-hexene units in the crystallites.[41,42] Larger 1-alkene comonomers, such as 1-octene, are unable to cocrystallize with the propene units at any level[40] and are therefore included in Figure 7 for an extended composition range. At a fixed X_B content, the same variation of ΔH as for T_{mp} with type of counit was observed. PB and PE exhibit higher heat of fusion due to the accommodation of the counits in the crystallites and the concomitantly large concentration of crystalline sequences that participate in the crystallization process. Since the 1-hexene, l-octene, and (3,1)-associated defects are not cocrystallizing units, one expects polypropylenes with these counits to have lower heat of fusion with respect to PE and PB copolymers. The experimental data of Figure 7 fulfill this expectation. What is again surprising in some respect is the dramatic depression of (3,1) *i*PP heat of fusion with respect to the PO and PH values, especially at the higher defect contents. At ∼3 mol %, the (3,1) *i*PP ΔH decreases only by ∼12% (from ∼80 to 70 J/g) and by >80% (from ∼30 to 5 J/g) at 15 mol % defects. ΔH becomes almost zero in *rac*-**1** *i*PP with ∼17 mol % defects, while at the same defect level the ΔH of the PO and PH copolymers is ∼15 J/g. Clearly, due to differences in isotactic sequence lengths, (3,1) *i*PP samples lose crystallinity at a much greater rate than PO or PHs with a matched point defect composition.

The impact of the (3,1) units on crystallinity calculated from the heat of fusion ($\Delta H/209$) is displayed comparatively with values for PH and PO copolymers in Figure 8; thus, the behavior of counits rejected from the crystalline regions is directly compared. Here, the DSC-based weight fraction crystallinity values are normalized by the weight fraction of crystalline units (f_w) to account for the difference in weight of the 1-hexene and 1-octene counits, as well as the a−f defect units. Clearly, even after this normalization, a large difference in crystallinity remains. The crystallinity level of *rac*-**1** *i*PP drops about 15% at the lowest defect content and decreases by 85%, from 19% for PO to ∼4% for *rac*-**1** *i*PP at a 14 mol % defect level. This large decrease in crystallinity content cannot be explained by molecular weight differences. It is well-established for homopolymers[58−61] as well as random copolymers[56] that the level of crystallinity decreases with increasing molecular weight. Therefore, from molecular weight differences, we would expect *rac*-**1** *I*PP to have higher (not lower as observed) crystallinites. The higher molar *mass* of the *rac*-**4** *i*PP compared with the *rac*-**1** *i*PP could explain the ∼5% lower crystallinity for the rac-**4** *i*PP. However, differences in isotactic run length in the range of high defect content (Figure 4) could also explain the lower crystallinity level of *rac*-**4** *i*PP5.93 and *i*PP8.11.

As with the melting points, the crystallinity of the *rac*-**4** *i*PP samples with the lowest defect content are anomalously high.

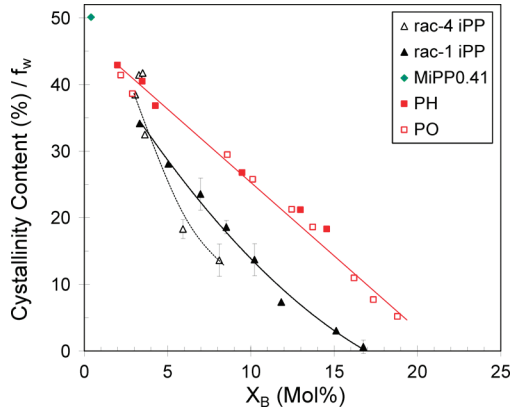

Figure 8. DSC crystallinity normalized by weight fraction of crystalline monomers vs point defect composition for random propylene−1-alkene copolymers and *i*PP with chain-walking defects. The continuous lines are added only as guides of the variation of experimental data.

One possible explanation is that these polymers may have nonhomogeneous interchain defect composition distribution. For example, if a population of chains has 2 mol % defects and the remaining chains have 4 mol % defects, then the average NMR composition may be the observed 3.3 mol %. The crystallites formed from chains with 2 mol % will melt at higher temperatures and display, on average, higher crystallinities than the chains with 4 mol %. Interchain compositional heterogeneities are commonly tested by temperature rising elution fractionation (TREF).[62] In this technique, a dilute solution of the copolymer is slowly crystallized to generate a distribution of crystallite thicknesses on the basis of chain composition. A subsequent increase of the elution temperature generates a profile of dissolution temperatures according to crystallite thicknesses. Narrow and single-peaked profiles are associated with a homogeneous interchain composition, while broad or multimodal profiles correspond to compositions that differ from chain to chain. The TREF profiles of (3,1) *i*PP are narrow and single-peaked, instead of broad and multimodal, as expected for heterogeneous copolymers (for the *rac*-**4** *i*PP3.51 example profile, see Figure S3 in the Supporting Information). Narrow TREF profiles rule out compositional heterogeneities as the origin of the anomalous high melting.

A second explanation is that temperature fluctuations during polymerization or spatial inhomogeneities in the polymerization mixture may have caused intrachain defect composition fluctuations in these samples. Such effects will be more relevant in *i*PP synthesized with the more active *rac*-**4** catalyst. Intrachain defect composition fluctuations due to changes in the catalyst activity with polymerization time were tested by taking an aliquot (6 h, entry 2, Table 1) and comparing with the final polymer sample (48 h, entry 1, Table 1). The defect content, melting temperature, and degree of crystallinity are basically the same and therefore independent of polymerization time. The anomalous behavior of low-defect *rac*-**4** *i*PP remains thus unexplained.

Further evidence of the drastic decrease in (3,1) *i*PP crystallinity level in reference to copolymers with noncrystallizable counits was obtained from WAXD patterns. Selected sample sets with about the same defect content (∼3, ∼8, and ∼10 mol %) are comparatively studied in Figure 9 for samples that were slowly cooled from the melt to ambient temperature (∼2 °C/min). The major differences in type of reflection and intensity between (3,1) *i*PP and PH or PO copolymers occur for defect content >5 mol %. (3,1) *i*PP displays less intense, broader

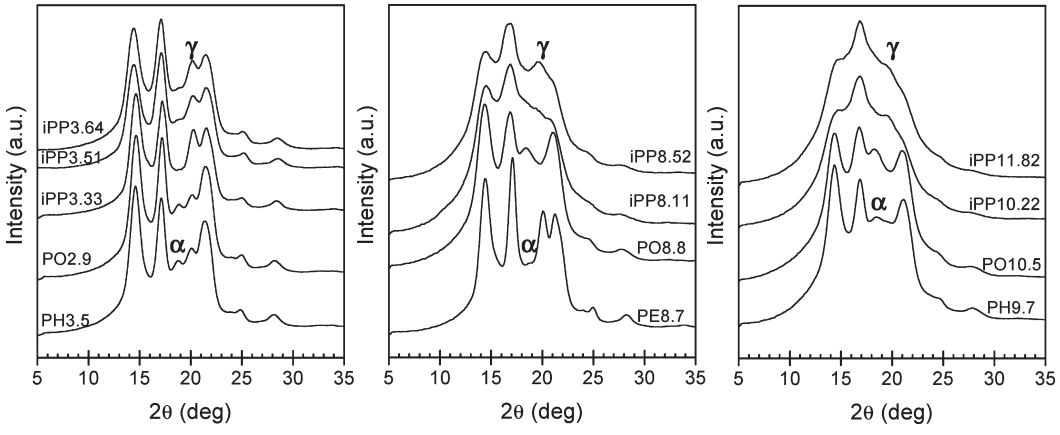

Figure 9. WAXD diffractograms of *i*PP and 1-alkene copolymers slowly cooled from the melt to ambient temperature. Diffractograms are shown at comparative defect levels of ∼3.5, 8.5, and ∼10.5 mol %.

dx.doi.org/10.1021/ma200231a |*Macromolecules* 2011, 44, 3436–3451

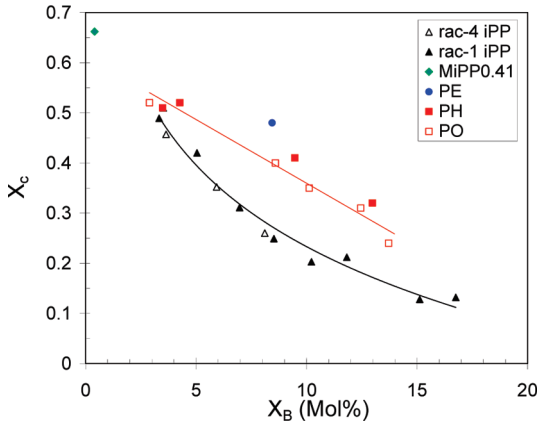

Figure 10. Degree of crystallinity calculated from WAXD patterns as a function of the total defect content (mol %) for *i*PP with chain-walking defects and 1-alkene copolymers. The continuous lines are guides for the variation of experimental data.

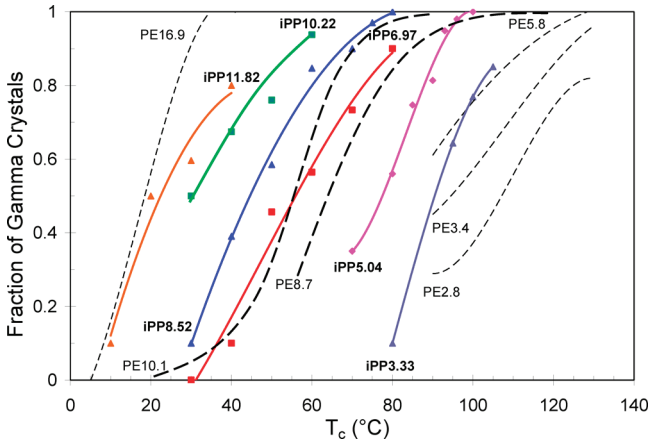

Figure 11. Content of γ crystals developed as a function of increasing isothermal crystallization temperature. Dashed lines are for propylene−ethylene (PE) copolymers (from ref 39) and solid lines data for (3,1) *i*PP.

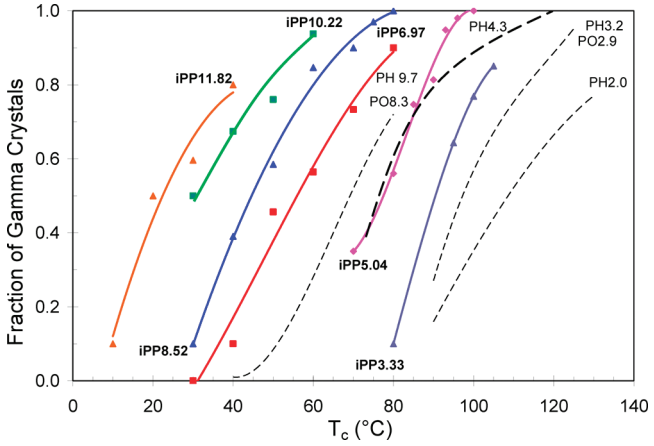

Figure 12. Content of γ crystals developed as a function of increasing isothermal crystallization temperature. Dashed lines are for propylene−1-hexene (PH) and propylene−1-octene (PO) copolymers (from ref 40) and solid lines data for (3,1) *i*PP.

reflections, indicating a lower crystalline fraction. The crystallinity levels obtained after subtraction of the amorphous pattern are portrayed in Figure 10. The difference in crystallinity between *rac*-**1** and *rac*-**4** *i*PP is not as evident from this data; however, a large crystallinity decrease with respect to values of PH and PO copolymers remains, which is similar to the DSC crystallinities. (3,1) *i*PP exhibit about half of the copolymer's crystallinity at ≥10 mol % defects. This dramatic decrease in crystallinity of (3,1) *i*PP is a consequence of the shortening of the isotactic crystallizable sequences by (3,1)-associated defects, which is more prevalent at increasing overall defect concentrations. WAXD crystallinities are ∼10% higher than the values derived from DSC due to a contribution of the crystal−amorphous interfacial region having crystal-like scattering but a liquid-like enthalpy.[55,63]

3.4. Polymorphism and Crystallite Thicknesses. Extensive studies on *i*PP and random l-alkene copolymers synthesized with metallocene catalysts have demonstrated that the presence of defects in the *i*PP chain favors the formation of the γ (orthorhombic) polymorph over the more common α (monoclinic) phase.[32−34] For *i*PP with the most common stereodefects and (2,1) regiodefects, the content of γ crystals is favored in polypropylenes with shorter isotactic sequence lengths. As the content of randomly distributed defects increases, the crystallizable sequence length decreases and polypropylenes tend to crystallize with a higher content of the γ phase.[32,33] The effect of the comonomer on shortening isotactic sequences, and hence in the formation of the γ polymorph, depends strongly on the level of inclusion of the comonomer and the strain in the crystal lattice.[39−41] When the counits are excluded from the crystal, such as PH (<13 mol %) and PO random copolymers, the average length of crystallizable sequences is equivalent; hence, PH and PO develop the same content of γ phase.[33,40] The (3,1)-associated defects are also excluded from the crystallites; however, their average isotactic sequence lengths are shorter than for PH or PO copolymers with equivalent point defect concentration. One then expects higher contents of γ phase in (3,1) *i*PP in consonant with differences in backbone defect microstructure. The diffractograms of Figure 9 give qualitative evidence of the differences in isotactic sequence length. At a content of defects of ∼3.5 mol %, PH and PO display reflections at 18.8° (α) and 20.1° (γ), while under the same crystallization conditions, (3,1) *i*PP crystallize mainly in the γ polymorph. The α reflection is basically absent in the (3,1) *i*PP diffractograms. Quantitative polymorphic studies were carried out on isothermally crystallized *rac*-**1** (3,1) *i*PP (for WAXD diffractograms see the Supporting Information, Figure S4). With increasing crystallization temperature, the content of the γ phase is compared with propylene−ethylene copolymers (Figure 11) as well as with PO and PH copolymers (Figure 12).[39,40]

The (3,1) *i*PP experimental data of Figure 11 are reconciled on the basis of isotactic sequence length partitioning due to the random nature of the defects. The content of γ phase developed by (3,1) *i*PP follows the trends of PE copolymers; i.e., fixing T_c, the content of γ increases with increasing defects due to a reduction of isotactic sequence length. The increase of γ with increasing T_c at fixed defect content is explained by an increased γ thermodynamic stability with respect to the α phase.[64] When comparing the polymorphic behavior for closely matched defect concentrations, large systematic differences are found between (3,1) *i*PP and PE. The content of γ phase of (3,1) *i*PP at any T_c is higher than in PE due to a large reduction of (3,1) *i*PP crystallizable

dx.doi.org/10.1021/ma200231a |*Macromolecules* 2011, 44, 3436–3451

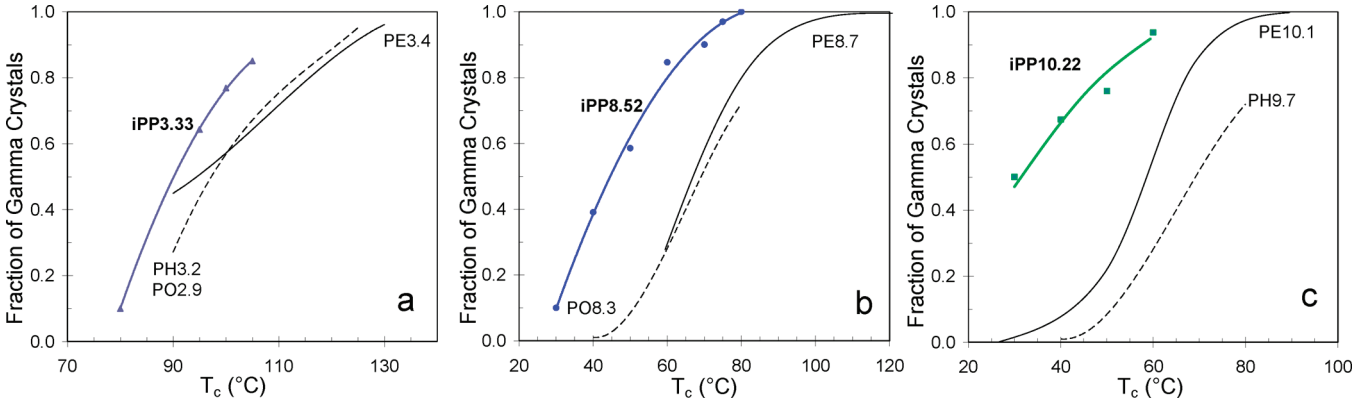

Figure 13. Effect of type of defect on content of γ crystals developed as a function of increasing isothermal crystallization temperature: (a) ~3.3 mol %, (b) ~8.5 mol %, and (c) ~10.1 mol %. Dashed lines are for propylene−1-hexene (PH) and propylene−1-octene (PO) copolymers (from ref 40) and solid lines data for PE (from ref 39) and (3,1) *i*PP.

sequence lengths from two superimposed effects. One is associated with the partial accommodation of the ethylene unit in the α and γ crystals which nominally increases the length of backbone crystalline sequences in PE with respect to (3,1) *i*PP that have noncrystallizable ethylene runs. The second is the additional reduction of (3,1) *i*PP isotactic sequence length due to chain straightening caused by (3,1) associated defects. The higher the defect content is, the more pronounced are these two effects leading to a larger difference in % γ (Figure 11). For example, fixing defect content at ~3.5 mol % and T_c at 100 °C, PE and (3,1) *i*PP develop 55% and 75% γ, respectively (a 20% difference in γ). Upon increasing defect content to 10.2 mol % at a T_c of 50 °C, the γ content is 25% for PE and 80% for (3,1) *i*PP (the γ difference increases to 55%).

(3,1) *i*PP also develops much higher contents of γ phase than PH and PO copolymers, regardless of the exclusion of the counits (comonomer or chain walking defects) from the crystallites (Figure 12). For instance, at T_c = 60 °C, the percentage of γ of *i*PP8.52 and PO8.5 is 85% and 27%, respectively, or a 3 times increase of (3,1) *i*PP γ crystals due to chain straightening and the concomitant reduction in average isotactic sequence length. A more direct comparison of the effect of (3,1)-associated defects with PE, PH, and PO copolymers is given in Figure 13. In this figure, the content of γ phase with increasing T_c is portrayed for sets with ~3.3, ~8.5, and ~10.1 mol % defects. Clearly, in the whole range of defect concentration, (3,1) *i*PP develops much higher contents of γ phase than any l-alkene random copolymer with matched defect content. The γ difference between (3,1) *i*PP and copolymers increases with increasing the overall content of defects.

A subject of interest concerning the trends of γ content for PH or PO copolymers in Figure 13 is that the general structural requirement of short crystallizable sequences favoring the formation of the γ polymorph does not hold for these two types of copolymers with >8 mol % defects. The crystallizable sequences of PO8.3 and PH9.7 are shorter than for PE8.7 or PE10.1, yet the γ fraction of the former is about the same (figure 13b) or lower (Figure 13c). Furthermore, the γ phase does not develop in PO and PH, with >13 mol % defects, while γ reaches ~100% in PE and (3,1) *i*PP with equivalent defect content. Lack of formation of γ phase in PO and PH in this range of defects is clearly not due to differences in partitioning of the defect, since the (3,1)-associated defects are also rejected from the lattice. The polymorphic

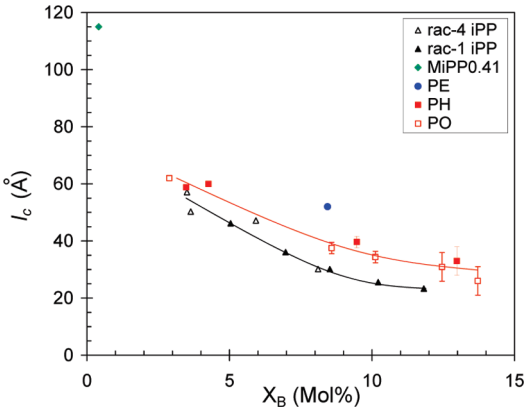

Figure 14. Crystallite thicknesses as a function of the total defect content (mol %) for *i*PP with chain-walking defects and propylene/1-alkene copolymers.

data suggest that the length of the branch in PH and PO is interfering with the required homoepitaxy for γ formation.

Crystallite thicknesses obtained from SAXS long periods, corrected with the crystallinity fraction derived by WAXD, are given in Figure 14 for slowly cooled specimens. Below ~4 mol %, the crystallite thicknesses of (3,1) *i*PP and PH/PO copolymers are very similar (~55 Å). Conversely, the influence of b, c, or d bulky defects and additional backbone carbons from (3,1) insertions displaces the crystallite thicknesses to increasingly thinner values as the overall content of chain-walking defects increases. As expected, PE8.7 displays higher crystal thickness. Hence, the reduction of the crystallizable sequence length in *i*PP with chain-walking, compared to matched random copolymers, also affects crystallite thicknesses in a manner that follows the decrease of melting points measured by DSC.

3.5. Analysis of Melting Temperatures and Level of Crystallinity Following Equilibrium Theory. All experimental evidence points to a (3,1) *i*PP defect microstructure consistent with shorter isotactic sequences compared with matched molar composition PH or PO copolymers. This includes the decrease in melting temperatures, levels of crystallinity, and crystallite thicknesses as well as the development of higher contents of γ phase. Up to the present, all comparative analyses have been carried out

dx.doi.org/10.1021/ma200231a |*Macromolecules* 2011, 44, 3436–3451

using a customary percentage of point defects over 100 monomers (X_B). Next, we evaluated whether the melting temperatures and degree of crystallinity follow the behavior of PH and PO copolymers if the analysis of the experimental data is carried out on the basis of total crystalline and noncrystalline point units instead of total monomer units. This implies taking the isotactic monomers as crystalline units and the chain-walking defects a−f as noncrystalline units and computing the crystalline content on a total unit basis. In this manner, the experimental data can be tested for conformity with Flory's exclusion equilibrium theory.

According to Flory's theory, the equilibrium melting temperature of a copolymer with crystallizable units and randomly distributed noncrystallizable units (T_m) relative to that of the homopolymer (T_m^o) can be expressed as[65]

$$\frac{1}{T_m} - \frac{1}{T_m^{\,o}} = -\frac{R}{\Delta H_u} \ln p \qquad (1)$$

Here ΔH_u is the enthalpy of fusion per repeating unit and p is the crystalline sequence propagation probability. For a random copolymer, p is identified with the mole fraction of crystallizable units. For counits of different size, p is replaced by the crystalline molar volume fraction. Equation 1 implies that the variation in the melting temperature−composition relation should not depend on the chemical nature of the counit for random copolymers, provided the counits do not cocrystallize with the isotactic units. The melting temperatures of copolymers are crucially dependent on the sequence distribution, which is associated with the value of p. If the isotactic sequence distribution of (3,1) *i*PP follows random statistics, as expected, then their melting temperature−composition relation plotted on the basis of p should follow the behavior of PH and PO copolymers. The value of p for the copolymer is identified with X_A or crystallizable units over total units (the total units are point defects plus crystallizable monomers). The effect of chain straightening in (3,1) *i*PP is taken into account, correcting the value of X_A by the additional backbone carbons due to (3,1)-associated defects. For (3,1) *i*PP, $p = Y_A$ is calculated as

$$Y_A = \frac{2X_A}{2X_A + \sum\left(3a + \frac{8}{3}b + \frac{6}{2}c + \frac{5}{2}d + 2f + 2st\right)} \qquad (2)$$

In eq 2 crystallizable monomers and defects are considered as units as indicated above, and we take into account the different number of backbone carbons in a crystallizable unit or in a chain-walking defect unit per monomer. For example, there are two carbons per crystallizable monomer, three carbons per (3,1) insertion, eight carbons per three monomer units that make defect b, etc.

The melting temperatures plotted according to eq 1 are shown in Figure 15, where the T_m vs composition format, $(1 - X_A)$ for copolymers or $(1 - Y_A)$ for (3,1) *i*PP, is maintained in order to facilitate comparison with data of Figure 6. The *i*PP melting data closely follow the melting behavior of PO and PH. The small shift to higher T_m values for *rac*-**1** *i*PP is explained by their lower molecular weights. These data demonstrate that when chain-walking defects are considered as units and their effect in reducing the content of crystallizable units is taken into account, the melting behavior of (3,1) *i*PP follows the dictates of equilibrium theory. Therefore, we can conclude that the generation of chain-walking defects by MAO-activated living Ni(II) α-diimine complexes in propylene polymerization follows the random statistics

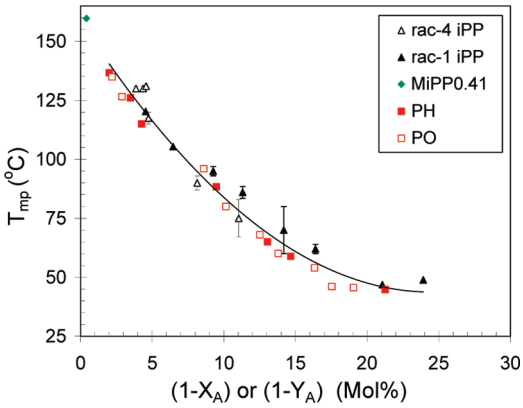

Figure 15. Melting temperatures vs percent of defect units, $(1 - X_A)$ for random copolymers (PO, PH) and $(1 - Y_A)$ for (3,1) *i*PP. The continuous line is an average over all the data points.

of the earlier metallocene catalysts. The difference in crystallizable sequence length explains the observed lower melting of (3,1) *i*PP in Figure 6 when compared with earlier metallocene *i*PP or copolymers on a total monomer molar defect composition basis.

Next, we analyzed the predicted effect of a backbone bulky defect, such as type b, on the theoretical equilibrium degree of crystallinity in reference to crystallinity values for *i*PP with single inverted units (for example, the (2,1) defect) and propylene−1-octene copolymers. The 1-octene comonomer unit was chosen because it has a molecular weight similar to the value of the b defect. Put another way, the b and 1-octene defects have similar volume fraction, but while the first adds eight defect carbons to the chain backbone, the 1-octene adds only two. Flory's thermodynamic equilibrium theory for the crystallization of random copolymers puts restrictions on the fraction of crystallizable units that can participate in the crystallization at a given temperature (T).[65] Only crystals made of sequences with a number of consecutive crystalline units above n^* are stable at T. n^* is calculated as[55,65]

$$n^* = -\frac{1}{\theta + \ln p}\left[\ln\left(\frac{DX_A}{p}\right) + 2\ln\left(\frac{(1-p)}{1-e^{-\theta}}\right)\right] \qquad (3)$$

$$\text{with} \quad \theta = \frac{\Delta H_u}{R}\left(\frac{1}{T} - \frac{1}{T_m^{\,o}}\right) \quad \text{and} \quad D = e^{-2\sigma_e a_o/RT} \qquad (4)$$

T_m^o is the melting point for the pure crystal (459.1 K), ΔH_u the enthalpy of fusion per pure crystalline unit (2100 cal/mol =2 × 10^9 erg/cm^3), σ_e the basal free energy (96 erg/cm^3), and a_o the cross-sectional area of a polypropylene chain (2.05 × 10^5 m^2 mol^{-1}).[39] The weight fraction equilibrium crystallinity is given as[55,65]

$$f_c = \frac{\frac{f_w}{p}(1-p)^2 p^{n^*}\left[\frac{p}{(1-p)^2} - \frac{e^{-\theta}}{(1-e^{-\theta})^2} + n^*\left[\frac{1}{(1-p)} - \frac{1}{(1-e^{-\theta})}\right]\right]}{1 - \frac{f_w}{p}p^{n^*}\left[\frac{1-p}{1-e^{-\theta}}\right]^2 [n^*(1-e^{-\theta}) + e^{-\theta}]} \qquad (5)$$

here f_w is the weight fraction of crystallizable units, which is equivalent to the volume fraction of crystallizable units in the molten polymer with the assumption that the density of crystallizable and noncrystallizable units in the melt is equivalent. The

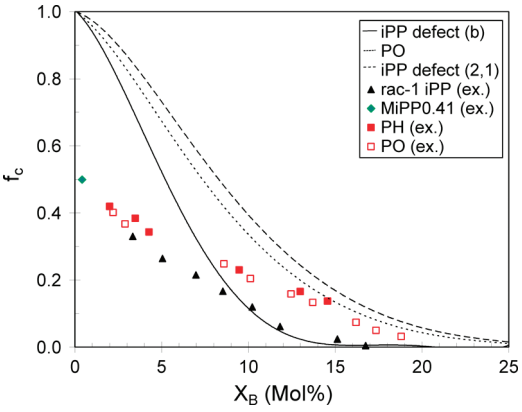

Figure 16. Comparison of equilibrium crystallinity to experimental values from DSC. Equilibrium lines calculated for *i*PP with chain-walking defects of type b (solid line), random propylene−1-octene copolymers (dotted line), and *i*PP with (2,1) defects (dashed line). Experimental data: propylene−1-hexene copolymers (closed squares), propylene−1-octene copolymers (open squares), *rac*-**1** *i*PP(closed triangles), and *i*PP with (2,1) defects (closed diamond).

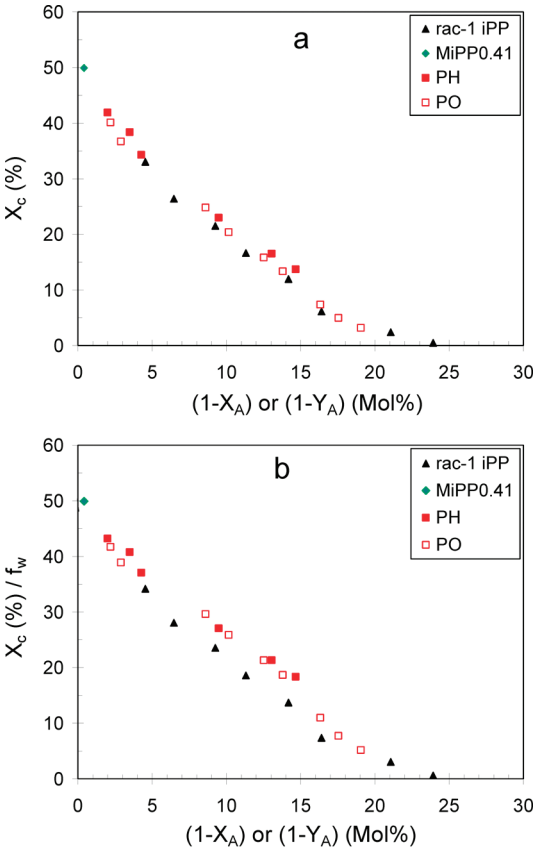

Figure 17. (a) DSC crystallinity vs percent of defect units for random copolymers (PO, PH) and *rac*-**1** *i*PP with chain-walking defects. (b) DSC crystallinity content normalized by weight fraction of crystalline monomers vs percent of defect units for random copolymers (PO, PH) and *rac*-**1** *i*PP with chain-walking defects.

crystallizable sequence probability, p, is identified with X_A or with Y_A for *i*PP with chain-walking defects as discussed above.

Equilibrium crystallinities (f_c) are plotted along with the DSC crystallinity in Figure 16. In reference to the (2,1) defect, the effect of a larger (PO) unit on f_w is to decrease crystallinity by about 5% in the range of defect concentration of interest (up to 20 mol %). In contrast, the effect of a multimonomer unit, such as the b defect, in f_w and p causes a decrease of crystallinity that depends on the content of b units. At low defect contents, the decrease in crystallinity by chain straightening beyond the decrease caused by the 1-octene or (2,1) units is small, less that 10% difference up to ∼3 mol % defects. (3,1) *i*PP crystallinity shifts progressively to much lower values for higher defect contents. For example, equilibrium considerations predict that (3,1) *i*PP with 10 mol % b defects will result in a 75% reduction of crystallinity level (from 40% to 10%) in reference to *i*PP with (2,1) regiodefects. The predicted crystallinity decrease at a 15 mol % defect composition is ∼80%, or from 17% to 3% crystallinity. While PO copolymers and (2,1) *i*PP display some equilibrium crystallinity at defect concentrations as high as 25 mol %, *i*PP with long backbone b defects lose crystallinity at much lower defect concentrations. For (3,1) *i*PP with 17 mol % b defects, the calculated crystallinity is less than 1%. Given that the molar mass of the b defect is similar to that of the 1-octene comonomer, the dramatic crystallinity loss is due mainly to the multimonomer character of the b defect with eight backbone carbons per unit instead of two carbons.

The experimental increasing gap in crystallinity between (3,1) *i*PP and PO copolymers with increasing defect concentration is thus explained from an equilibrium basis. The effect of lowering the (3,1) *i*PP content of crystalline sequences with $n > n^*$, with respect to the copolymer or (2,1) *i*PP, is minor at defect levels <2 mol % but becomes quite large when the defect concentration increases, due to the higher number of long defected runs restricting the (3,1) *i*PP crystallizable isotactic sequence length. Although equilibrium and experimental data follow a very similar pattern, the absolute crystallinity values differ greatly in the low concentration range due to kinetic and topological restraints on the equilibrium expectation, as amply discussed in previous works.[63,66−68]

The experimental and calculated crystallinity values become similar for >10 mol % defects. This unexpected feature was also found in ethylene copolymers[68] and is attributed in part to the low equilibrium crystallinity levels that highly defected copolymers have at room temperature and to a crystalline sequence distribution that is more sharply peaked for short isotactic sequences.[55,68]

In discussing the melting behavior, we surmised that (3,1) *i*PP crystallites and the crystals from propylene−l-alkene copolymers have the same melting temperature composition relation when plotted on the basis of $(1 - Y_A)$ or $(1 - X_A)$. A similar plot for the degree of crystallinity obtained from heat of fusion brings the data to a common curve (Figure 17a). When unit defect composition (point defects over all units) instead of molar composition (point defects over total monomer units) is analyzed, the crystallization of *i*PP with chain-walking defects follows the dictates of Flory's exclusion theory, as expected for defects with sizes too large to be accommodated in the *i*PP crystal lattice. The crystallinity level of (3,1) *i*PP is ∼5% lower than PO copolymers, when the weight fraction of crystalline monomers is considered (Figure 17b), which is the opposite behavior than is expected due to molecular weight difference. Somewhat lower crystallinity points out that the bulky nature of chain-walking defects adds additional restraints to diffusing crystalline sequences through the entangled melt to the growing crystal front. It is also plausible that *i*PP with (3,1) enchainments have a more restricted registry of segmental helices of the required handness for crystallization,

dx.doi.org/10.1021/ma200231a |*Macromolecules* 2011, 44, 3436–3451

especially when a large number of a and d type defects are generated. We notice that the perpetuation of a (3,1) helical symmetry through these two types of defects (Scheme 4) will cause a change from a right-handed to left-handed segmental helix. Compared to *i*PP chains with defects free from this helical switching, the development of crystallinity may be more hindered, especially at low crystallization temperatures (the region where defect-rich *i*PP crystallize), for which the melt chain dynamics are slower.

4. CONCLUDING REMARKS

Polypropylenes synthesized with MAO-activated living nickel α-diimine catalysts have complex, unique defect microstructures. Chain-walking events resulting in (3,1) enchainments can be controlled by the reaction temperature and to some extent by the type of catalyst ligand. The defect microstructure of two *i*PP series synthesized with *rac*-**1** and *rac*-**4** has been fully characterized by ^{13}C NMR spectroscopy. Five different defect structures have been identified at different levels in all *i*PP generated with these catalysts. Most defects are isolated or are successive groups of (2,1) inversions and (3,1) enchainments. At a fixed reaction temperature and time, the cumyl-derived catalyst, *rac*-**4**, propagates chain growth more efficiently and adds lower concentration of defects, which leads to *i*PP with higher molar masses and higher isotacticity. Moreover, at a fixed point defect concentration, *rac*-**4** *i*PP has a higher content of bulky defects and, therefore, shorter average isotactic runs than *rac*-**1** *i*PP. This is reflected in lower melting temperatures and lower crystallinity contents for the *rac*-**4** *i*PP.

The thermodynamic and structural properties of these polypropylene samples have been comparatively studied in reference to earlier metallocene *i*PP and copolymers used as control. Specifically, random *i*PP copolymers with comonomers excluded from the crystalline regions, such as the PH and PO copolymers, were examined in a range of defect composition between 3 and ∼20 mol %. On a customary point defect molar composition based on 100 monomers, *i*PP with chain-walking defects were found to melt at lower temperatures and display a dramatic depression of crystallinity at defect levels of 8−15 mol %. These features, coupled with lower crystallite thicknesses and enhanced contents of crystallites in the γ phase, are associated with a shortening of isotactic sequence lengths, which are caused by the bulky nature of most (3,1)-associated defects when compared with random copolymers. Chain-walking defects, such as (3,1) enchainments, decrease the level of *i*PP crystallinity at a much faster rate than the more common defects found in Ziegler−Natta or early metallocene-made *i*PP as well as propylene random 1-alkene copolymers.

The melting behavior and crystallinity contents are also analyzed on the basis of Flory's equilibrium theory by computing the crystalline content out of crystalline plus noncrystalline units that are found in 100 monomer units. The addition of three carbons to the chain backbone, instead of two, by the (3,1) enchainment was also taken into account. Plotted on this basis, the melting temperature−composition behavior closely follows the behavior of PH and PO random copolymers. It is then concluded that although chain-walking adds ethylene runs to the *i*PP chain, these defects are excluded from the crystallite regions and are generated in the synthesis following random statistics. Moreover, the multimonomer nature of some of the defects as well as the addition of three carbons, instead of two, to the chain backbone causes additional restraints to the development of crystallinity. Even after accounting for the shorter crystallizable sequences in (3,1) *i*PP, crystallinity remains slightly lower than for matched random copolymers.

■ ASSOCIATED CONTENT

Supporting Information. Detailed ^{13}C NMR characterization of defect microstructure and equations for quantitative analysis, ^{13}C DEPT spectrum of *i*PP8.11, TREF profile for *rac*-**4** *i*PP3.51, and powder WAXD diffractograms of isothermally crystallized *rac*-**1** *i*PPs. This material is available free of charge via the Internet at http://pubs.acs.org.

■ AUTHOR INFORMATION

Corresponding Author
*E-mail: alamo@eng.fsu.edu.

■ ACKNOWLEDGMENT

Funding of this work by the National Science Foundation (DMR-0706205) is gratefully acknowledged. We thank C. J. Ruff of ExxonMobil Chemical Co. for measurements and help with solution ^{13}C NMR analysis, D. Lohse of ExxonMobil Research and Engineering Co. for TREF measurements and the Florida Advanced Center for Composite Technologies (FAC^{2}T) for access to the center's X-ray instrumentation. This research made use of the Cornell Center for Materials Research Shared Experimental Facility supported through the NSF MRSEC program (DMR-0520404).

■ REFERENCES

(1) Chum, P. S.; Swogger, K. W. *Prog. Polym. Sci.* **2008**, *33*, 797–819.
(2) Scheirs, J.; Kaminsky, W., Eds. *Metallocene-Based Polyolefin*; Wiley: Chichester, 2000, Vol. 2.
(3) Brintzinger, H. H.; Fischer, D.; Mulhaupt, R.; Rieger, B.; Waymouth, R. M. *Angew. Chem., Int. Ed. Engl.* **1995**, *34*, 1143–1170.
(4) Arriola, D. J.; Carnahan, E. M.; Hustad, P. D.; Kuhlman, R. L.; Wenzel, T. T. *Science* **2006**, *312*, 714–719.
(5) Wang, H. P.; Khariwala, D. U.; Cheung, W.; Chum, S. P.; Hiltner, A.; Baer, E. *Macromolecules* **2007**, *40*, 2852–2862.
(6) Khariwala, D. U.; Taha, A.; Chum, S. P.; Hiltner, A.; Baer, E. *Polymer* **2008**, *49*, 1365–1375.
(7) Coates, G. W.; Waymouth, R. M. *Science* **1995**, *267*, 217–219.
(8) Witte, P.; Lal, T. K.; Waymouth, R. M. *Organometallics* **1999**, *18*, 4147–4155.
(9) Cherian, A. E.; Rose, J. M.; Lobkovsky, E. B.; Coates, G. W. *J. Am. Chem. Soc.* **2005**, *127*, 13770–13771.
(10) Killian, C. M.; Tempel, D. J.; Johnson, L. K.; Brookhart, M. *J. Am. Chem. Soc.* **1996**, *118*, 11664–11665.
(11) Gottfried, A. C.; Brookhart, M. *Macromolecules* **2001**, *34*, 1140–1142.
(12) Schmid, M.; Eberhardt, R.; Klinga, M.; Leskela, M.; Rieger, B. *Organometallics* **2001**, *20*, 2321–2330.
(13) Gottfried, A. C.; Brookhart, M. *Macromolecules* **2003**, *36*, 3085–3100.
(14) Hicks, F. A.; Jenkins, J. C.; Brookhart, M. *Organometallics* **2003**, *22*, 3533–3545.
(15) Camacho, D. H.; Guan, Z. *Macromolecules* **2005**, *38*, 2544–2546.
(16) Rose, J. M.; Cherian, A. E.; Coates, G. W. *J. Am. Chem. Soc.* **2006**, *128*, 4186–4187.
(17) Wild, L.; Blatz, C. Development of High Performance TREF for Polyolefins Analysis. In *New Advances in Polyolefins*; Chung, T. C., Plenun Press: New York, 1993.

(18) Watkins, J. J.; Krukonis, V. J.; Condo, P. D.; Pradhan, D.; Ehrlich, P. *J. Supercrit. Fluids* **1991**, *4*, 24–31.
(19) Busico, V.; Cipullo, R. *Prog. Polym. Sci.* **2001**, *26*, 443–533.
(20) Virkkunen, V.; Laari, P.; Pitkanen, P.; Sundholm, F. *Polymer* **2004**, *45*, 3091–3098.
(21) Busico, V.; Cipullo, R.; Polzone, C.; Talarico, G.; Chadwick, J. C. *Macromolecules* **2003**, *36*, 2616–2622.
(22) Shroff, R. N.; Mavridis, H. *Macromolecules* **2001**, *34*, 7362–7367.
(23) Vega, J. F.; Santamaria, A.; Munoz-Escalona, A.; Lafuente, P. *Macromolecules* **1998**, *31*, 3639–3647.
(24) Ittel, S. D.; Johnson, L. K.; Brookhart, M. *Chem. Rev.* **2000**, *100*, 1169–1203.
(25) Guan, Z.; Cotts, P. M.; McCord, E. F.; McLain, S. J. *Science* **1999**, *283*, 2059–2062.
(26) Guan, Z. *J. Polym. Sci., Part A: Polym. Chem.* **2003**, *41*, 3680–3692.
(27) McCord, E. F.; McLain, S. J.; Nelson, L. T. J.; Arthur, S. D.; Coughlin, E. B.; Ittel, S. D.; Johnson, L. K.; Tempel, D.; Killian, C. M.; Brookhart, M. *Macromolecules* **2001**, *34*, 362–371.
(28) Galland, G. B.; da Silva, L. P.; Dias, M.; Crossetti, G. L.; Ziglio, C. M.; Filgueiras, C. A. *J. Polym. Sci: Part A: Polym. Chem.* **2004**, *42*, 2171–2178.
(29) Rose, J. M.; Deplace, F.; Lynd, N. A.; Wang, Z.; Hotta, A.; Lobkovsky, E. B.; Kramer, E. J.; Coates, G. W. *Macromolecules* **2008**, *41*, 9548–9555.
(30) Hotta, A.; Cochran, E.; Ruokolainen, J.; Khanna, V.; Fredrickson, G. H.; Kramer, E. J.; Shin, Y.-W.; Shimizu, F.; Cherian, A. E.; Hustad, P. D.; Rose, J. M.; Coates, G. W. *Proc. Natl. Acad. Sci. U. S. A.* **2006**, *103*, 15327–15332.
(31) Deplace, F.; Wang, Z.; Lynd, N. A.; Hotta, A.; Rose, J. M.; Hustad, P. D.; Tian, J.; Ohtaki, H.; Coates, G. W.; Shimizu, F.; Hirokane, K.; Yamada, F.; Shin, Y.-W.; Rong, L.; Zhu, J.; Toki, S.; Hsiao, B. S.; Fredrickson, G. H.; Kramer, E. J. *J. Polym. Sci., Part B: Polym. Phys.* **2010**, *48*, 1428–1437.
(32) Alamo, R. G.; Kim, M.-H.; Galante, M. J.; Isasi, J. R.; Mandelkern, L. *Macromolecules* **1999**, *32*, 4050–64.
(33) Hosier, I. L.; Alamo, R. G.; Esteso, P.; Isasi, J. R.; Mandelkern, L. *Macromolecules* **2003**, *36*, 5623–36.
(34) (a) De Rosa, C.; Auriemma, F.; Circelli, T.; Waymouth, R. M. *Macromolecules* **2002**, *35*, 3622–3629. (b) De Rosa, C.; Auriemma, F.; Spera, C.; Talarico, G.; Tarallo, O. *Macromolecules* **2004**, *37*, 1441–1454. (c) De Rosa, C.; Auriemma, F.; Di Capua, A.; Resconi, L.; Guidotti, S.; Camurati, I.; Nifant'ev, I. E.; Laishevtsev, I. P. *J. Am. Chem. Soc.* **2004**, *126*, 17040–17049. (d) De Rosa, C.; Auriemma, F.; Paolillo, M.; Resconi, L.; Camurati, I. *Macromolecules* **2005**, *38*, 9143–9154.
(35) Thomann, R.; Wang, C.; Kressler, J.; Mülhaupt, R. *Macromolecules* **1996**, *29*, 8425–8434.
(36) (a) Brückner, S.; Meille, S. U.; Petraccone, U.; Pirozzi, B. *Prog. Polym. Sci.* **1991**, *16*, 361–404. (b) Thomann, R.; Semke, H.; Maier, R. D.; Thomann, Y.; Scherbe, J.; Mülhaupt, R.; Kressler, J. *Polymer* **2001**, *42*, 4597–4603.
(37) Rieger, B.; Mu, X.; Mallin, D. T.; Rausch, M. D.; Chien, J. C. W. *Macromolecules* **1990**, *23*, 3559–3568.
(38) (a) Alamo, R. G.; VanderHart, D. L.; Nyden, M. R.; Mandelkern, L. *Macromolecules* **2000**, *33*, 6094–6105. (b) VanderHart, D. L.; Alamo, R. G.; Nyden, M. R.; Kim, M.-H.; Mandelkern, L. *Macromolecules* **2000**, *33*, 6078–6093. (c) Nyden, M. R.; Vanderhart, D. L.; Alamo, R. G. *Comput. Theor. Polym. Sci.* **2001**, *11*, 175–189.
(39) Jeon, K.; Chiari, Y. L.; Alamo, R. G. *Macromolecules* **2008**, *41*, 95–108.
(40) Jeon, K.; Palza, H.; Quijada, R.; Alamo, R. G. *Polymer* **2009**, *50*, 832–844.
(41) (a) De Rosa, C.; Auriemma, F.; Ruiz de Ballesteros, O.; Resconi, L.; Camurati, I. *Macromolecules* **2007**, *40*, 6600–6616. (b) De Rosa, C.; Auriemma, F.; Talarico, G.; Ruiz de Ballesteros, O. *Macromolecules* **2007**, *40*, 8531–8532. (c) De Rosa, C.; Auriemma, F.; Ruiz de Ballesteros, O.; De Luca, D.; Resconi, L. *Macromolecules* **2008**, *41*, 2172–2177. (d) De Rosa, C.; Auriemma, F.; Ruiz de Ballesteros, O.; Resconi, L.; Camurati, I. *Chem. Mater.* **2007**, *19*, 5122–30.
(42) (a) Poon, B.; Rogunova, M.; Hiltner, A.; Baer, E.; Chum, S. P.; Galeski, A.; Piorkowska, E. *Macromolecules* **2005**, *38*, 1232–1243. (b) Lotz, B.; Ruan, J.; Thierry, A.; Alfonso, G. C.; Hiltner, A.; Baer, E.; Piorkowska, E.; Galeski, A. *Macromolecules* **2006**, *39*, 5777–5781.
(43) Meille, S. V.; Brückner, S. *Nature (London)* **1989**, *340*, 455–457.
(44) Turner-Jones, A.; Aizlewwod, J. M.; Beckett, D. R. *Makromol. Chem.* **1964**, *75*, 134–158.
(45) Soga, K.; Shiono, T. *Makrom. Chem. Rapid Commun.* **1987**, *8*, 305–311.
(46) Cheng, H. N. *Macromolecules* **1984**, *17*, 1950–1955.
(47) Kuo, J.-C.; Lin, W.-F.; Yu, C.-H.; Tsai, J.-C.; Wang, T.-C.; Chung, T.-M.; Ho, R.-M. *Macromolecules* **2008**, *41*, 7967–7977.
(48) Asakura, T.; Nishiyama, Y.; Doi, Y. *Macromolecules* **1987**, *20*, 616–620.
(49) Zhou, Z.; Stevens, J. C.; Klosin, J.; Kümmerle, R.; Qiu, X.; Redwine, D.; Cong, R.; Taha, A.; Mason, J.; Winniford, B.; Chauvel, P.; Montañez, N. *Macromolecules* **2009**, *42*, 2291–2294.
(50) Senda, T.; Hanaoka, H.; Hino, T.; Oda, Y.; Tsurugi, H.; Mashima, K. *Macromolecules* **2009**, *42*, 8006–8009.
(51) Carman, C. J.; Harrington, R. A.; Wilkes, C. E. *Macromolecules* **1977**, *10*, 536–544.
(52) De Rosa, C.; Auriemma, F.; Di Capua, A.; Resconi, L.; Guidotti, S.; Camurati, I.; Nifant'ev, I. E.; Laishevtsev, I. P. *J. Am. Chem. Soc.* **2004**, *126*, 17040–17049.
(53) Randall, J. C. *Polymer Sequence Determination. Carbon 13-NMR Method*; Academic Press: New York, 1977.
(54) Alizadeh, A.; Richardson, L.; Xu, J.; McCartney, S.; Marand, H.; Cheung, Y. W.; Chum, S. *Macromolecules* **1999**, *32*, 6221–6235.
(55) Crist, B.; Howard, P. R. *Macromolecules* **1999**, *32*, 3057–3067.
(56) Alamo, R. G.; Chan, E. K. M.; Mandelkern, L.; Voigt-Martin, I. G. *Macromolecules* **1992**, *25*, 6381–6394.
(57) Hser, J. C.; Carr, S. H. *Polym. Eng. Sci.* **1979**, *19*, 436. Mathot, V. B. F.; Piipers, M. F. J. *Polym. Bull.* **1984**, *11*, 297–304.
(58) Mandelkern, L. *J. Phys. Chem.* **1971**, *75*, 3909–3920.
(59) Mandelkern, L.; Allou, A. L., Jr.; Gopalan, M. *J. Phys. Chem.* **1968**, *72*, 309–318.
(60) Alamo, R. G.; Blanco, J. A.; Agarwal, P.; Randall, J. C. *Macromolecules* **2003**, *36*, 1559–1571.
(61) Xu, J.; Feng, L.; Yang, S.; Yang, Y.; Kong, X. *Eur. Polym. J.* **1998**, *34*, 431–434.
(62) Mingozzi, I.; Cecchin, G.; Morini, G. *Int. J. Polym. Anal. Charact.* **1997**, *3*, 293–317.
(63) Alamo, R.; Domszy, R.; Mandelkern, L. *J. Phys. Chem.* **1984**, *88*, 6587–6595.
(64) Ferro, D. R.; Brückner, S.; Meille, S. V.; Ragazzi, M. *Macromolecules* **1992**, *25*, 5231–5235.
(65) Flory, P. J. *Trans. Faraday Soc.* **1955**, *51*, 848–856.
(66) Alamo, R.; Mandelkern, L. *Thermochim. Acta* **1994**, *238*, 155–201.
(67) Alamo, R.; Mandelkern, L. *Macromolecules* **1991**, *24*, 6480–6493.
(68) Crist, B.; Finerman, T. M. *Polymer* **2005**, *46*, 8745–8751.